[9–11]. Among these cell types, adult skin fibroblasts are a desirable potential source of somatic cells, since they can be clinically accessed without ethical problems. To help devise future clinical transplantation therapies, it is necessary to determine which iPSCs derived from tail-tip fibroblasts (TTFs) (adult skin fibroblasts in mice) are most fit to generate HSCs.

Previously, we reported variation in hematopoietic potential among several iPSC lines, regardless of the source of somatic cells [12]. This observation suggested that variation in hematopoietic potential could occur among TTF-derived iPSCs. To address this issue, we analyzed mesodermal and hematopoietic potential in five TTF-derived iPSC lines established using different transcription factors (*Oct3/4, Sox2* and *Klf4* with or without *c-Myc*) or reporter genes (*DsRed* or *GFP*). We demonstrate that both mesodermal and hematopoietic cell number and expression of mesoderm and hematopoietic cell differentiation markers varies among the five lines. Interestingly, 212B2 iPSCs, the only line created via *c-Myc* transduction, exhibited lower capacity to differentiate into mesodermal and hematopoietic cells compared than did the other four iPSCs.

Materials and Methods

iPSCs Maintenance

We used the five lines of tail-tip fibroblast (TTF)-derived iPSCs, such as 256H13, 256H18, 212B2, 212D1 and 335D1, which were kindly provided by Dr. Shinya Yamanaka (Kyoto University). These iPSCs were established by "separate method" as previously described [6]. Briefly, pMX-Oct3/4, pMX-Klf4, pMX-Sox2, and/or pMX-c-Myc plasmids were separately transfected into separate dishes of Plat-E cells using Fugene 6 reagent (Roche Applied Science, Indianapolis, IN). Twenty-four hours after transfection, the medium was replaced with serum-containing DMEM. After 24 h, each virus-containing supernatant was mixed and used for retroviral infection. Concerning iPSCs generation, TTFs were isolated from adult Nanog-GFP-IRES-Puro^r reporter mice or adult DsRed-transgenic mice. For the four-factor transduction, retrovirus-containing supernatants for *Klf4*, *c-Myc*, *Oct3/4*, *Sox2* and *DsRed*, were mixed with the ratio of 1:1:1:1:4. When the fibroblasts were transduced with the three factors, retrovirus-containing supernatants for *Klf4*, *Oct3/4*, *Sox2*, *DsRed* and Mock were mixed with the ratio of 1:1:1:1:4. For transfection, TTFs were seeded at 8.0×10^5 cells in 100-mm dish, without feeder cells. TTFs were incubated in the virus/polybrene-containing supernatants for 24 h. Four days after transduction, TTFs transduced with the three factors were reseeded at 3.5×10^5 cells per 100-mm dish with SNL feeder cells and cultured with ES medium containing DMEM, 15% FBS, 0.1 mM non essential amino acid, 0.1 mM 2-mercaptoethanol (2-ME) and 1000U/ml mouse leukemia inhibitory factor (LIF). TTFs transduced with the four factors were reseeded at 0.5×10^5 cells per 100-mm dish with feeder cells. Thirty to forty days after transduction, the colonies were selected for expansion. Drug selection with puromycin (1.5 μg/ml) was done for 212B2, 212D1 and 335D1 iPSCs. 256H13 and 256H18 iPSC lines were established without drug selection [6]. Twenty to thirty percent efficiency was achieved in transfection of all five iPSC lines.

We firstly expanded these iPSC lines with mitomycin-C (MMC)-treated mouse embryonic fibroblasts (MEFs) in StemMedium (DS Pharma Biomedical, Hyogo, Japan) containing 0.1 mM 2-ME (Nacalai Tesque, Inc., Kyoto, Japan) and 1000 U/ml mouse LIF (prepared in Dr. Minetaro Ogawa's Laboratory). The passage number (P) for each line used in this study was as follows; 256H13 (P.6-P.9), 256H18 (P.8-P.10), 212B2 (P.9), 212D1 (P.6), and 335D1 (P.8-P.10).

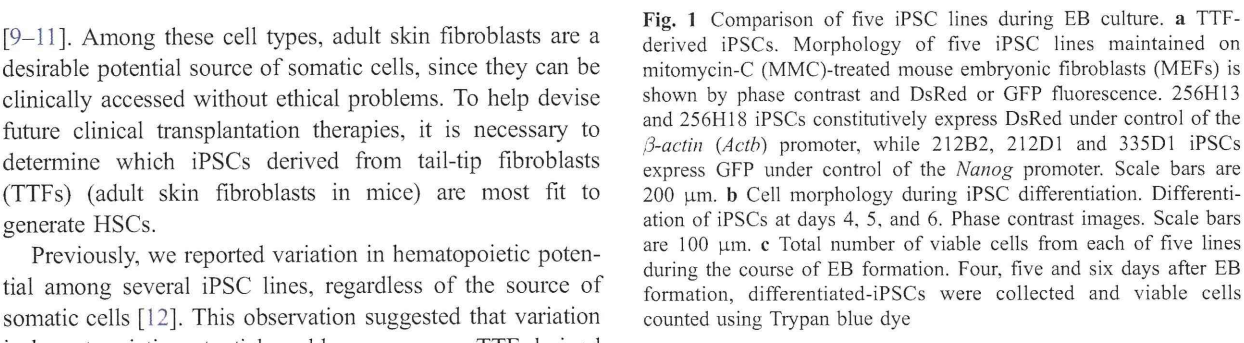

Fig. 1 Comparison of five iPSC lines during EB culture. **a** TTF-derived iPSCs. Morphology of five iPSC lines maintained on mitomycin-C (MMC)-treated mouse embryonic fibroblasts (MEFs) is shown by phase contrast and DsRed or GFP fluorescence. 256H13 and 256H18 iPSCs constitutively express DsRed under control of the *β-actin* (*Actb*) promoter, while 212B2, 212D1 and 335D1 iPSCs express GFP under control of the *Nanog* promoter. Scale bars are 200 μm. **b** Cell morphology during iPSC differentiation. Differentiation of iPSCs at days 4, 5, and 6. Phase contrast images. Scale bars are 100 μm. **c** Total number of viable cells from each of five lines during the course of EB formation. Four, five and six days after EB formation, differentiated-iPSCs were collected and viable cells counted using Trypan blue dye

Embryoid Body (EB) Formation

Before EB formation, iPSCs were separated from feeder cells by 0.5-hour incubation to eliminate the attached MEF cells. Then, iPSCs expressing stage-specific embryonic antigen-1 (SSEA-1) were purified by magnetic cell separation (MACS, Miltenyi Biotec, Auburn, CA). iPSCs (6×10^4 cells) were cultured in 3 ml of EB medium, which contains Iscove's Modified Dulbecco's Medium (IMDM, SIGMA-ALDRICH, St. Louis, MO) containing 15% FBS (a pre-selected batch showing the highest efficiency in inducing hematopoietic cells), 2 mM L-glutamine (SIGMA-ALDRICH), 0.0026% (vol/vol) monothioglycerol (MTG; Wako Pure Chemical Industries, Osaka, Japan), 50 μg/ml L-ascorbic acid (Wako Pure Chemical Industries), 10 U/ml penicillin, and 10 μg/ml streptomycin (SIGMA-ALDRICH).

For mesodermal cell differentiation, no cytokine was added in the EB medium. Petri dishes (60-mm in diameter, Kord-Valmark™, Ontario, Canada) were used to generate EBs. On culture days 4, 5, and 6, cells were collected by gentle pipetting, washed once in PBS, and then incubated in

a

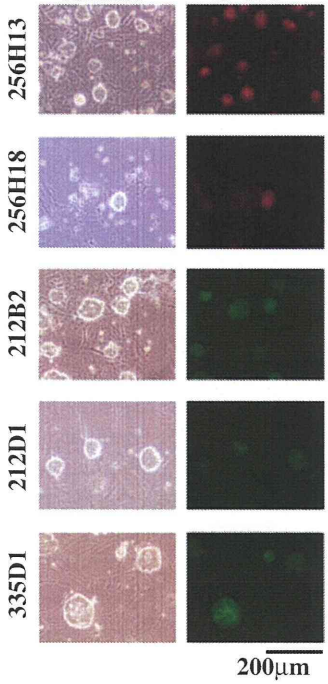

iPSC line	Transduced genes	Reporter gene	Transduction method	Viral vector	Genetic selection
iPS-TTF-FB/DsRed-256H13	Oct3/4, Klf4, Sox2	Actb-DsRed	Retrovirus	pMX-Oct3/4 pMX-Klf4 pMx-Sox2	w/o
iPS-TTF-FB/DsRed-256H18	Oct3/4, Klf4, Sox2	Actb-DsRed	Retrovirus	pMX-Oct3/4 pMX-Klf4 pMX-Sox2	w/o
iPS-TTF-FB/Ng-212B2	Oct3/4, Klf4, Sox2, c-Myc	Nanog-GFP	Retrovirus	pMX-Oct3/4 pMX-Klf4 pMX-Sox2 pMX-c-Myc	Nanog
iPS-TTF-FB/Ng-212D1	Oct3/4, Klf4, Sox2	Nanog-GFP	Retrovirus	pMX-Oct3/4 pMX-Klf4 pMX-Sox2	Nanog
iPS-TTF-FB/Ng-335D1	Oct3/4, Klf4, Sox2	Nanog-GFP	Retrovirus	pMX-Oct3/4 pMX-Klf4 pMX-Sox2	Nanog

b

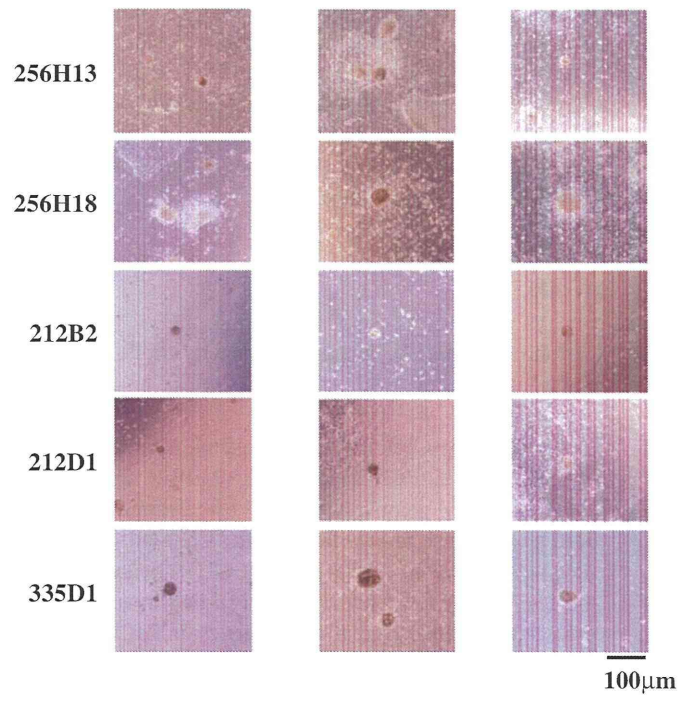

c

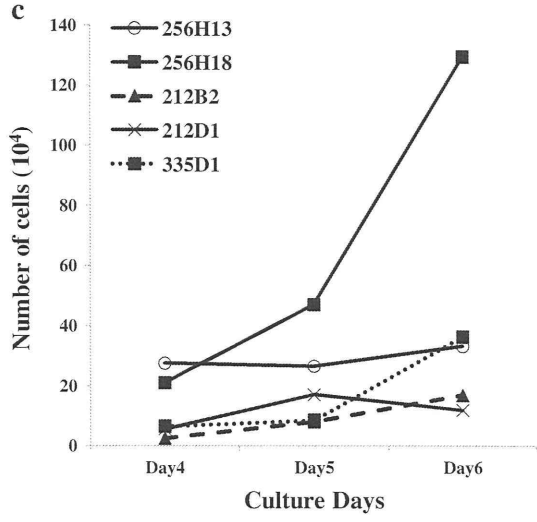

Cell Dissociation Buffer (Life Technologies, Carlsbad, CA) at 37°C for 30 min. An equal volume of medium containing 10% FBS was added and mixed gently by pipetting, and the cell suspension was passed through a 40-μm nylon mesh. The number of living cells was determined by staining with 0.4% Trypan blue (Life Technologies). For hematopoietic cell differentiation, SCF (stem cell factor), IL (interleukin)-3, EPO (erythropoietin), IL-6 and G-CSF (granulocyte colony-stimulating factor) were added in the EB medium. Petri dishes were used to generate EBs. On culture days 9, cells were collected and counted as mentioned above.

Flow Cytometry

To analyze mesodermal cells from iPSCs, cells cultured for 4, 5, and 6 days were collected as mentioned in 'EB formation' and stained with an APC-conjugated anti-CD324 (E-cadherin) antibody (Ab) (Alexa Fluor®647, eBioscience, San Diego, CA), a Pacific Blue™ -conjugated anti-mouse Flk1 (VEGFR2) Ab (BioLegend, San Diego, CA), a biotin-conjugated anti-mouse CD140α (PDGFRα) Ab (eBioscience) and an APC-Cy7-conjugated streptavidin (BD Biosciences, San Jose, CA). Biotin-conjugated antibody was used as a primary antibody and fluorescence-conjugated streptavidin was used as a secondary reagent, respectively. E-cadherin$^-$/Flk1$^+$ cells were defined as lateral mesodermal cells and E-cadherin$^-$/PDGFRα$^+$ cells as paraxial mesodermal cells, respectively.

To analyze hematopoietic cells from iPSCs, cells cultured for 9 days were collected as mentioned in 'EB formation' section and stained with an APC-Cy7-conjugated anti-mouse Ter119 Ab (eBioscience), a PB-conjugated anti-mouse CD45 Ab (BioLegend), an APC-conjugated anti-mouse F4/80 (BioLegend), a biotin-conjugated anti-mouse Gr-1 Ab (eBioscience) and PE-Cy7-conjugated streptavidin (BD Biosciences). For Mac1 Ab, a PE-conjugated anti-mouse Mac1 Ab (BioLegend) was used for GFP-expressing iPSCs (212B2, 212D1, and 335D1). And a biotin-conjugated anti-mouse Mac1 Ab (eBioscience) and a PE-Cy7-conjugated streptavidin were used for DsRed-expressing iPSCs, respectively. Biotin-conjugated antibody was used as a primary antibody and fluorescence-conjugated streptavidin was used as a secondary reagent, respectively. Ter119 positive cells were defined as erythroid cells, CD45 positive cell as leukocytes, Mac1$^+$/F4/80$^+$ cells as macrophages and Gr-1$^+$/F4/80$^-$ cells as granulocytes, respectively.

To stain dead cells, propidium iodide (PI, Life Technologies, Eugene, Oregon) was used for GFP-expressing iPSCs, and TO-PRO®-1 iodide (Life Technologies) was used for DsRed-expressing iPSCs. Cells were analyzed using a FACS Aria cell sorter (Becton Dickinson, Franklin Lakes, NJ). Data files were analyzed using FlowJo software (Tree Star, San Carlos, CA).

Fig. 2 Mesodermal cell differentiation from iPSCs. **a** Flow cytometric analysis of mesodermal cells from all five iPSC lines at days 4, 5, and 6 during the course of EB culture. Lateral mesodermal cells were evaluated based on lack of expression of the surface marker E-cadherin (CD324, epithelial cadherin) and expression of Flk1 (CD309, VEGFR2) (*upper panel*). Paraxial mesodermal cells were evaluated based on lack of expression of E-cadherin and expression of PDGFRα (*lower panel*). **b** Quantitative real-time PCR analysis was used to detect the mesodermal markers *Flk1*, *Tbx6* and *Brachyury* at day 4 of EB culture. Data was normalized to *β-actin* expression

Quantitative Real-Time PCR

Total RNA was isolated with the RNAqueous-Micro Kit (Ambion, Austin, TX). A high-capacity cDNA Archive kit (Applied Biosystems, Foster City, CA) was used to synthesize cDNA from mRNA. mRNA levels were normalized to *β-actin* as an internal control. In real-time PCR, mRNA levels were analyzed by the SYBR Green method with gene-specific primers or Taqman probe methods. Genes analyzed by SYBR Green included *Oct3/4* (Fw; gcagctcagccttaagaacatgt, Rv; cgatttgcatatctcctgaaggt), *Klf4* (Fw; gaactcacacaggcgagaaacc, Rv; tcggagcgggcgaatt), *Sox2* (Fw; atcaggctgccgagaatcc, Rv; ctcaaactgtgcataatggagt taaaaa) and *Nanog* (Fw; caaaaccaaaggatgaagtgcaa, Rv; gtgctgagcccttctgaatca). *Oct3/4*, *Klf4*, and *Sox2* primer sets recognized both internal and external sequences. Mouse *β-actin* (Fw; gctctggctcctagcaccat, Rv; gccaccgatccacacagagt) served as an internal control. Genes analyzed using the Taqman probe (Applied Biosystems) included *Flk1* (Mm01222421_m1), *Brachyury* (Mm01318252_m1), *Tbx6* (Mm00441681_m1), *Gata1* (Mm01352636_m1), *Klf1* (Mm00516096_m1), *CD45* (Mm01293577_m1), *Csf1r* (Mm01266652_m1), *PU.1* (Mm00488142_m1), and *c-Myc* (Mm00487804_m1). Mouse *β-actin* (4352933E) served as an internal control.

Results

Morphology and EB Formation Capacity of TTF-derived iPSCs

In this study, we cultured 5 induced pluripotent stem cell (iPSC) lines—256H13, 256H18, 212B2, 212D1, and 335D1—which were established by different protocols from adult mouse tail-tip fibroblasts (TTF) [6]. The *DsRed* gene is downstream of the *β-actin* (*ACTB*) gene in 256H13 and 256H18 iPSCs, whereas *GFP* is downstream of *Nanog* and serves an indicator of pluripotency in 212B2, 212D1, and 335D1 iPSCs, as summarized in Fig. 1a. *Oct3/4*, *Klf4*, *and Sox2* genes were transduced into TTFs to establish all iPSC lines, while the 212B2 line was also transduced with *c-Myc*. All iPSC colonies exhibited round morphology and exhibited large nucleoli and low cytoplasmic content.

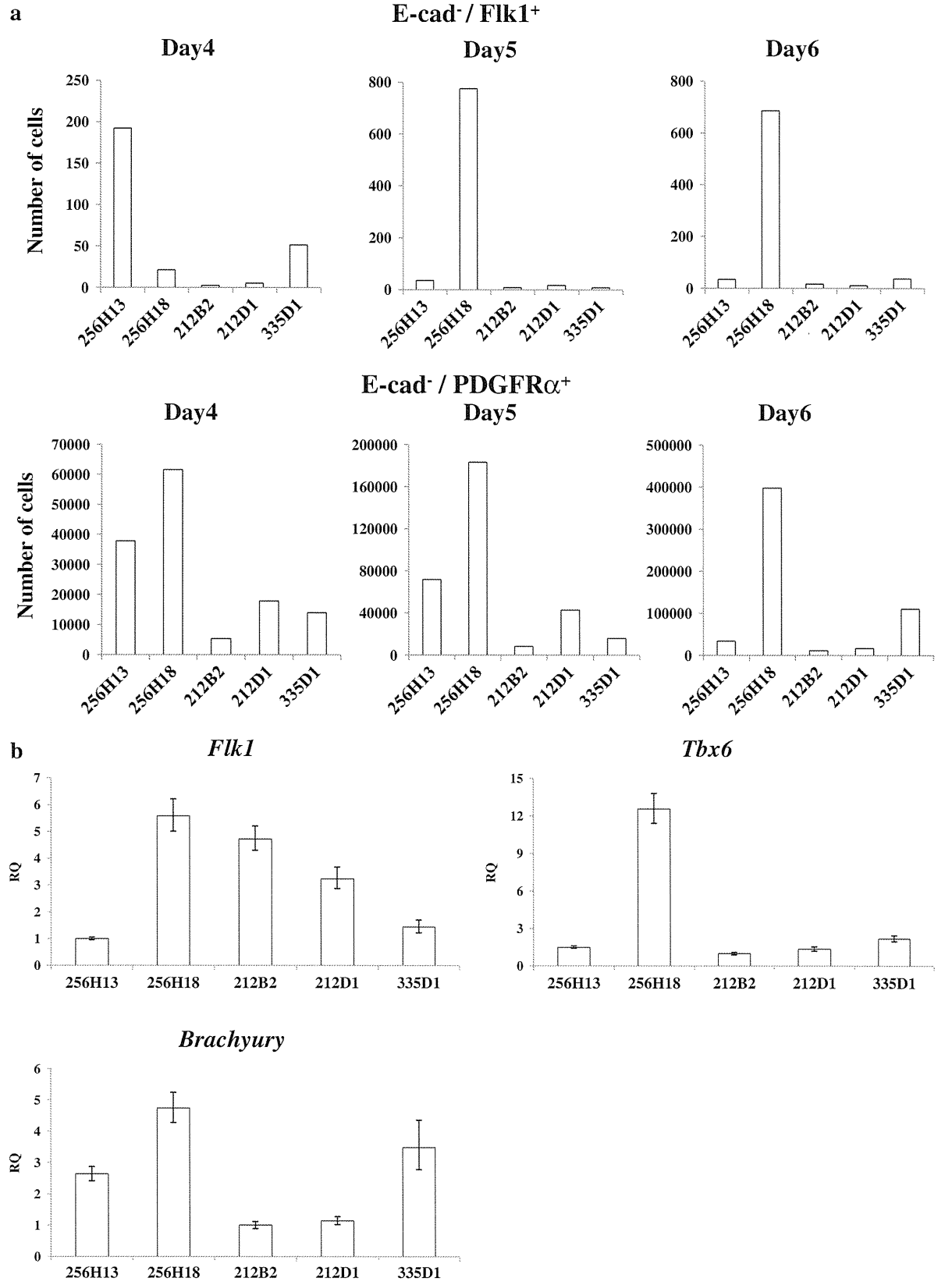
a
E-cad- / Flk1+
Day4
Day5
Day6
Number of cells
250
200
150
100
50
0
800
600
400
200
0
256H13
256H18
212B2
212D1
335D1
E-cad- / PDGFRα+
70000
60000
50000
40000
30000
20000
10000
200000
160000
120000
80000
40000
500000
400000
300000
200000
100000
b
Flk1
Tbx6
Brachyury
RQ
7
6
5
4
3
2
1
0
15
12
9
6
3

335D1 formed larger colonies than other lines (Fig. 1a). 212B2, 212D1and 335D1 lines were GFP-positive, indicative of *Nanog* expression and pluripotency.

Next, we performed differentiation culture using the method of embryoid body (EB) formation without cytokines (Supplementary Fig. 1a). Four, five and six days after EB formation, we observed the cultured cells microscopically (Fig. 1b) and evaluated proliferation by cell counting (Fig. 1c). All iPSCs formed EBs, although EB size and the number of adherent cells varied among lines (Fig. 1b). 212B2 and 335D1 iPSCs formed round EBs, although 335D1-derived EBs were larger than 212B2-derived EBs. By contrast, cultured 256H13, 256H18 and 212D1 iPSCs gave rise to adherent cells as well as round EBs. 256H18-derived EBs were larger than those derived from 212D1 cells at day 5 and, in the case of 256H18, adherent cells were observed most frequently (Fig. 1b). In terms of proliferation, the number of 256H13-derived cells increased at day 4 (2.75×10^5 cells) and then plateaued. The number of 256H18 iPSCs also increased gradually through the culture period and then plateaued. 256H18 iPSCs-derived cells gradually increased during the culture and plateaued at day 5 (4.70×10^5 cells). Although 212B2 and 335D1 lines increased gradually during the culture period, their viable cell number at day 6 (1.69×10^5 and 3.63×10^5, respectively) was lower than that of 256H18 iPSCs. By contrast, the number of 212D2-derived cells increased from day 4 (5.50×10^4 cells) to 5 (1.70×10^5 cells), and then decreased (1.19×10^5 cells). There was no significant difference among all iPSC lines in cell viability during EB culture (Supplementary Fig. 2). Taken together, our results indicate that EB formation and cell proliferation varies among five iPSC lines derived from the same tissue.

Mesodermal Potential of TTF-derived iPSCs

To assess iPSC hematopoietic potential, we first examined their mesodermal potential, as hematopoietic cells are mesodermal in origin [13, 14]. ESC mesodermal differentiation was monitored using three markers: lack of E-cadherin (a marker of both ectoderm and endoderm in early mouse development [15]) expression, expression of platelet-derived growth factor receptor α (PDGFRα) and Flk1 (also known as VEGF receptor 2) [16, 17]. We compared the number of iPSC-derived E-cadherin$^-$/Flk1$^+$ cells, representing lateral mesoderm, and E-cadherin$^-$/PDGFRα$^+$ cells, representing paraxial mesoderm, at days 4, 5 and 6 of EB culture, since ESC-derived EBs [18, 19] contain Flk1$^+$ mesodermal cells at 4 to 4.5 days of culture and iPSC-derived EBs contain Flk1$^+$ cells at 5 days of culture [12]. The emergence of E-cadherin$^-$/Flk1$^+$ cells from the 256H13 line was the most rapid among the five lines tested, and the number of cells in this fraction was highest at day 4 (193 cells) and then decreased (Fig. 2a, upper panel). The number of E-cadherin$^-$/Flk1$^+$ cells from 256H18 was the highest among the five lines tested (day 5; 776 cells) (Fig. 2a, upper panel). In contrast, the number of 212B2 and 212D1 iPSC-derived E-cadherin$^-$/Flk1$^+$ cells was lower than that seen in the other three lines. The number of E-cadherin$^-$/PDGFRα$^+$ cells from 256H18 was highest among the five lines (day 6; 3.97×10^5 cells) (Fig. 2a, lower panel). The number of E-cadherin$^-$/PDGFRα$^+$ cells from 256H13 and 212D1 lines increased from days 4 to 5 and then decreased, whereas those from 256H18 and 212B2 lines gradually increased from days 4 to 6. The number of E-cadherin$^-$/PDGFRα$^+$ cells from 335D1 dramatically increased from day 5 (1.59×10^4 cells) to day 6 (1.10×10^5 cells) (Fig. 2a, lower panel). To confirm iPSC mesodermal cell differentiation, we employed PCR to examine expression of the mesoderm markers *Flk1* (lateral mesoderm), *Tbx6* [20] (paraxial mesoderm) and *Brachyury* [21] (pan-mesodermal marker). *Flk1* expression was lowest in 256H13-derived cells at day 4 of culture (Fig. 2b), whereas it was highest in 256H18-derived cells over days 4 to 6 (Supplementary Fig. 3 and 5). *Tbx6* expression at day 4 was highest in 256H18-derived iPSCs, whereas *Tbx6* expression was highest at days 5 and 6 in 335D1- and 256H13-derived cells, respectively (Fig. 2b and Supplementary Fig. 3 and 5). *Brachyury* expression at day 4 was higher in 256H18- and 335D1-derived cells compared to others (Fig. 2b), whereas it was highest at days 5 and 6 in 335D1- and 256H13-derived cells, similar to *Tbx6* expression (Supplementary Fig. 3 and 5). There was a trend in mesodermal differentiation. Early differentiation in 256H13 cells was observed, whereas late differentiation in 335D1 (Fig. 2a). 256H18 cells differentiated into both lateral and paraxial mesoderm most frequently. Overall differences we observed in mesodermal differentiation potential suggest variation in mesodermal potential of adult skin-derived induced pluripotent stem cell lines in mice.

Fig. 3 Hematopoietic cell differentiation from iPSCs. **a** Differentiated iPSCs were collected at day 9 of EB culture and Ter119$^+$ erythroid cells were evaluated by flow cytometry. **b** Quantitative real-time PCR analysis was used to detect expression of the erythroid genes *Gata1* and *Klf1* at day 9 of EB culture. Data was normalized to *β-actin* expression. **c**, **d** Differentiated iPSCs were collected at day 9 of EB culture and evaluated by flow cytometry for (**c**) CD45$^+$ leukocytes and (**d**) myeloid cells (Mac1$^+$/F4/80$^+$ macrophages and Gr-1$^+$/F4/80$^-$ granulocytes). **e** Quantitative real-time PCR analysis was used to detect expression of the myeloid-related genes *CD45, Csf1r* and *PU.1* at day 9 of EB culture. Data was normalized to *β-actin* expression

Hematopoietic Potential of TTF-derived iPSCs

Next we examined cell number and the percentage of erythroid and myeloid cells emerging during EB formation at day 9 of culture in the presence of cytokines (Supplementary Fig. 1b). Flow cytometry analysis showed that

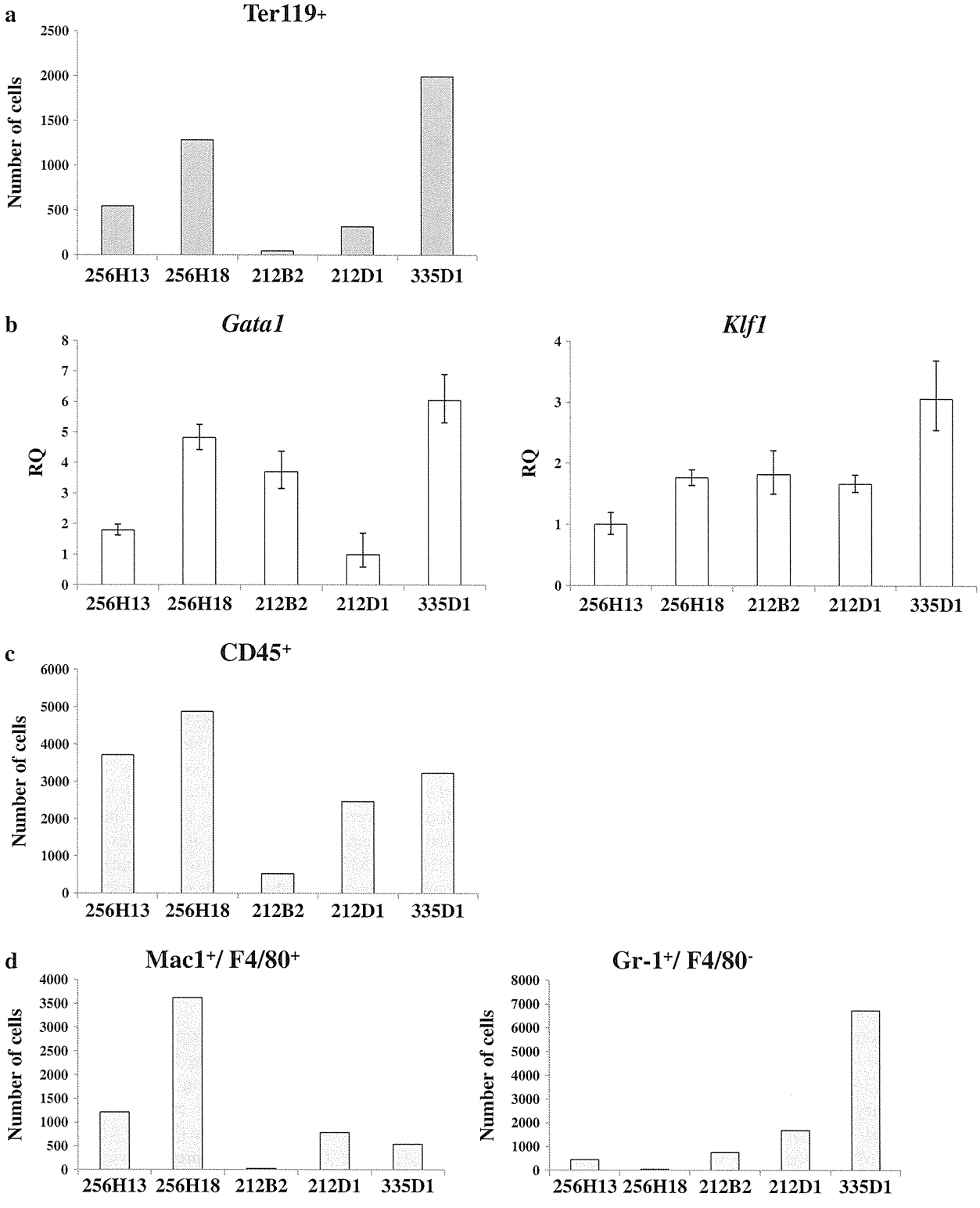
a
Ter119+
Number of cells
2500
2000
1500
1000
500
0
256H13
256H18
212B2
212D1
335D1
b
Gata1
RQ
8
7
6
5
4
3
2
1
0
256H13
256H18
212B2
212D1
335D1
Klf1
RQ
4
3
2
1
0
256H13
256H18
212B2
212D1
335D1
c
CD45+
Number of cells
6000
5000
4000
3000
2000
1000
0
256H13
256H18
212B2
212D1
335D1
d
Mac1+/ F4/80+
Number of cells
4000
3500
3000
2500
2000
1500
1000
500
0
256H13
256H18
212B2
212D1
335D1
Gr-1+/ F4/80-
Number of cells
8000
7000
6000
5000
4000
3000
2000
1000
0
256H13
256H18
212B2
212D1
335D1

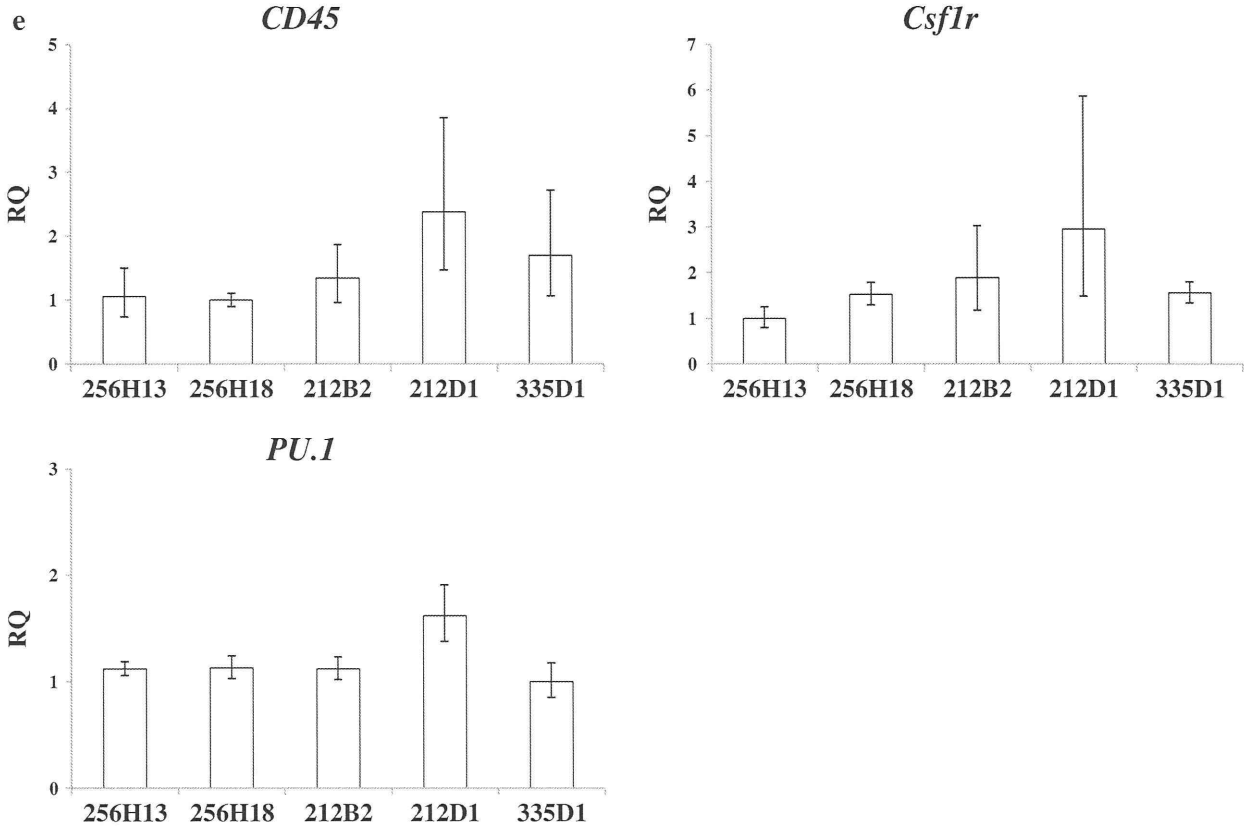

Fig. 3 (continued)

lines 256H18 and 335D1 efficiently differentiated into Ter119$^+$ erythroid cells at 0.35% (1280 cells) and 0.72% (1991 cells), respectively. By contrast, 212B2 cells differentiated into Ter119$^+$ cells at low frequency (46 cells, 0.12%) (Fig. 3a, Supplementary Fig. 4a). In agreement, real-time PCR analysis showed that expression of the erythropoietic transcription factors *Gata1* [22] and *Klf1* [23] was the highest in 335D1 cells (6.05 times higher than in 212D1 cells and 3.07 times higher than in 256H13 cells) (Fig. 3b). 256H18 and 335D1 cells differentiated into CD45$^+$ leukocytes at 1.32% (4880 cells) and 1.17% (3229 cells), respectively (Fig. 3c, Supplementary Fig. 4b).

Flow cytometry analysis showed that 256H18 cells differentiated into Mac1$^+$/F4/80$^+$ macrophages at high frequency (3622 cells, 0.98%) (Fig. 3d, left panel; Supplementary Fig. 4c, left panel), whereas 335D1 cells differentiated into Gr-1$^+$/F4/80$^-$ granulocytes at high frequency (6738 cells, 2.45%) (Fig. 3d, right panel; Supplementary Fig. 4c, right panel). By contrast, 212B2 cells, which are transduced with the *c-Myc* gene, differentiated into CD45$^+$ leukocytes, Mac1$^+$/F4/80$^+$ macrophages and Gr-1$^+$/F4/80$^-$ granulocytes at low frequency (523, 20 and 756 cells, respectively) (Fig. 3c, d). When we analyzed expression of the leukocyte marker *CD45*, *Csf1r* (encoding colony stimulating factor 1 receptor, a macrophage marker), and *PU.1* (also known as *Spi-1*, which marks the myeloid lineage) at culture day 9, no significant differences were observed among the five lines (Fig. 3e). Taken together, among the five iPSC lines tested, only 256H18 and 335D1 were capable of differentiating at high frequency into both erythroid cells and leukocytes at day 9 of culture.

Expression of Reprogramming and Pluripotency Genes During EB Formation from iPSCs

We next investigated whether pluripotency of iPSCs was related to the nature reprogramming factors used transduce somatic cells. Prior to initiating EB culture, *c-Myc* expression was highest in 212B2 cells, which had been transduced with *c-Myc* along with *Oct3/4*, *Klf4* and *Sox2* genes (Fig. 4a). *Oct3/4* gene expression was highest in 256H13 cells, whereas *Klf4*, *Sox2* and *Nanog* gene expression did not significantly differ among the lines prior to culture. *Oct3/4*, *Klf4* and *Sox2* expression at day 4 of culture was the highest in 212B2 cells, suggesting that they retain pluripotency longer than do the other lines (Fig. 4b).

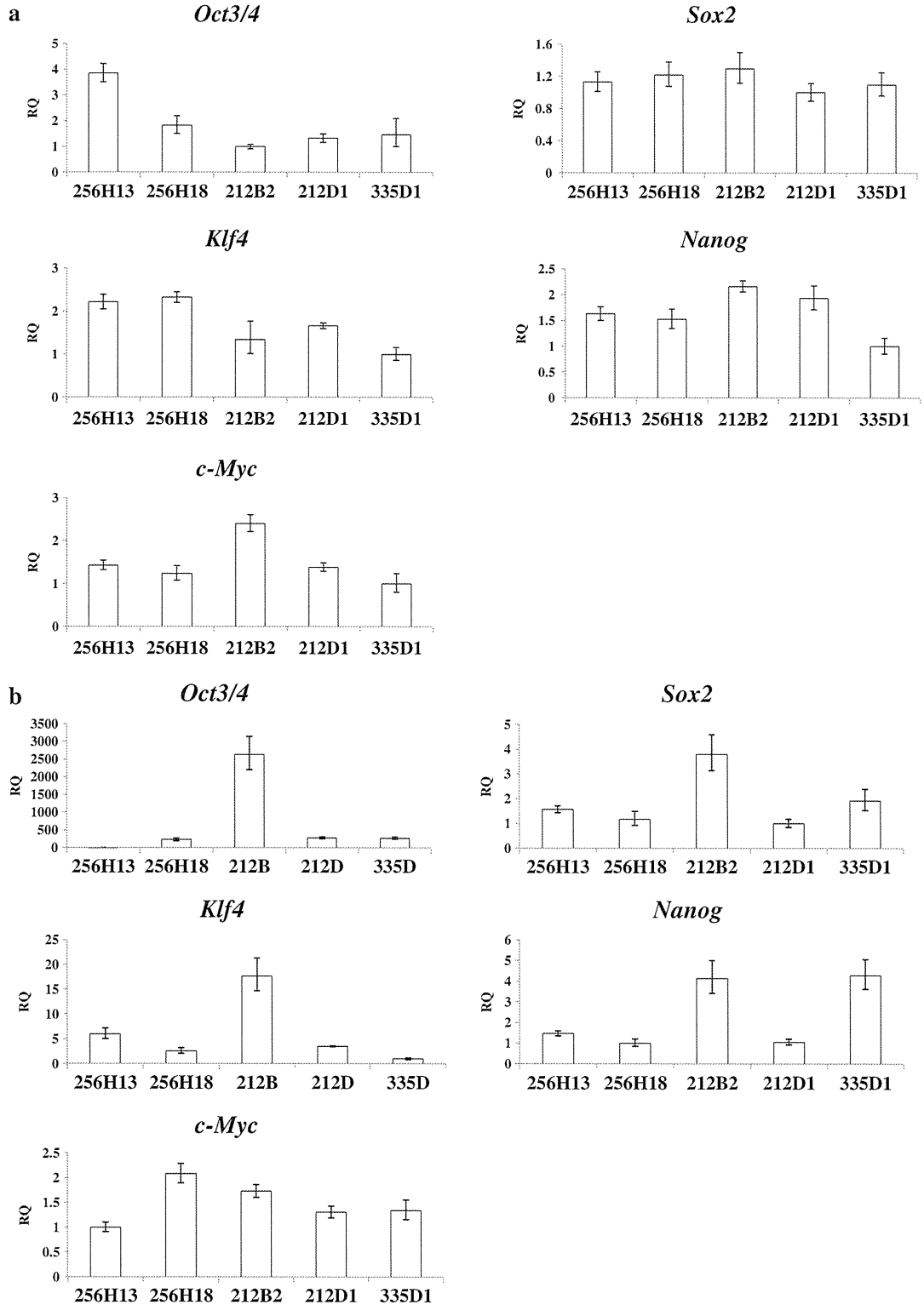

Fig. 4 Comparison of reprogramming and pluripotency gene expression. Quantitative real-time PCR analysis was used to detect expression of the reprogramming genes *Oct3/4, Klf4, Sox2* and *c-Myc* and the pluripotency gene *Nanog* at days 0 (**a**) and 4 (**b**) of EB culture. Data was normalized to *β-actin* expression

Discussion

iPSCs constitute important tools for future regenerative medicine. In this study we compared mesodermal and hematopoietic potential of several iPSC lines, since differentiation potential reportedly varies among iPSC lines established by different sources and methods [12]. Although all iPSCs possessed pluripotency, as defined by expression of *Oct3/4* and *Nanog*, each line showed variations in EB formation and cell proliferation. Examination of mesodermal potential using both flow cytometry and real-time PCR methods, confirmed these differences: specifically, the 256H18 iPSC line gave rise to mesodermal cells at high frequency, whereas 212B2 cells showed the lowest frequency. To identify factors underlying mesodermal potential, we compared expression of both differentiation and pluripotency markers. As summarized in Supplementary Fig. 5, expression of the differentiation markers *Flk1*, *Tbx6*, and *Brachyury* in 256H18 iPSCs was highest at day 4 of culture. Although there was no significant correlation between mesodermal potential and expression of pluripotency markers (Fig. 4), the number of EBs is likely positively correlated with mesodermal potential (Fig. 1). In terms of hematopoietic potential, variations in differentiation capacity were confirmed by flow cytometric and real-time PCR analyses. 256H18 and 335D1 iPSCs generated erythroid cells and leukocytes at high frequency, whereas a low frequency was seen with 212B2 cells (Fig. 3). Expression of the *Oct3/4*, *Sox2*, *Klf4* and *Nanog* pluripotency genes in 256H18 was lowest, whereas 212B2 iPSCs showed highest expression of *Oct3/4*, *Sox2* and *Klf4*. Given the results of our hematopoietic cell differentiation assays at day 4 of culture, these results suggest an inverse relationship between hematopoietic potential and pluripotency gene expression (Fig. 4). *c-Myc* expression in 212B2 cells was highest before culture (Fig. 4a), likely due to ectopic transduction of *c-Myc*. There was a correlation between high *c-Myc* expression and low induction of mesodermal and hematopoietic cells. In our culture conditions, *c-Myc* likely down-regulates mesodermal and hematopoietic cell induction from the 212B2 iPSC line. Our results are compatible with previous reports mentioning that *c-Myc* maintains pluripotency of ESCs [24] and iPSCs [25], and similar to the report showing that c-Myc down-regulates cardiogenic [26] and endodermal differentiation [25] of iPSCs. Taken together, our results imply that iPSCs lacking *c-Myc* transduction will be preferably used for clinical purposes.

Passage number of iPSCs reportedly affected the hematopoietic differentiation [27]. As passage number of iPSCs increased, the transient epigenetic memory of their original somatic cells was gradually lost and hematopoietic differentiation capacity was up-regulated in TTF-derived iPSCs [27]. 256H18 and 335D1 iPSCs generated hematopoietic cells at high frequency, whereas a low frequency was seen in 212B2 in our culture condition (Fig. 3). Since we used iPSC lines of 256H18, 335D1 and 212B2 with similar passage number (P.8- P.10), it is unlikely that passage number affected the hematopoietic differentiation capacity among these three lines. Concerning the other 2 iPSC lines, passage number was lower in 256H13 (P.6-P.9) and 212D1 (P.6) than in 256H18, 335D1 and 212B2. Less hematopoietic cell differentiation in 256H13 and 212D1 than 256H18 and 335D1 was might be due to the difference of passage number.

Taken together, even derived from the same TTF origin, each iPSC demonstrated different mesodermal and hematopoietic potential. Transduction method with retroviral infection and transfection efficiency (20–30%) were similar, while *c-Myc* gene transduction, drug selection with puromycin, reporter genes (Actb-DsRed or Nanog-GFP) and passage number were not identical among five iPSC lines. Therefore, variation in mesodermal and hematopoietic potential was likely affected by combination of transduced genes and passage number, but not transfection methods, drug selection and reporter genes.

Recently, it was reported that iPSCs can be established from peripheral blood (PB) cells [28]. Since collecting a PB sample from a patient is practically easier than taking skin fibroblasts by biopsy in terms of risk and pain, it will be further necessary to evaluate the hematopoietic potential of PB-derived iPSCs in both mice and humans.

Acknowledgements This work was supported by a grant from the Project for Realization of Regenerative Medicine from the Ministry of Education, Culture, Sports, Science and Technology and by a grant from the BASIS project from the Ministry of Education, Culture, Sports, Science and Technology. T. Inoue and K. Kulkeaw is supported by research fellowships from the Ministry of Education, Culture, Sports, Science and Technology, and from The Tokyo Biochemical Research Foundation, respectively. We thank Dr. Keisuke Okita, Ms. Yuka Horio, Ms. Chiyo Mizuochi and the Research Support Center, Graduate School of Medical Sciences, Kyushu University for technical supports, and Dr. Minetaro Ogawa and Dr. Hiroshi Sakamoto for providing LIF. All iPSCs were kindly provided by Dr. Shinya Yamanaka.

Author Contributions Tomoko Inoue performed the experiments, analyzed data and wrote the manuscript. Kasem Kulkeaw, Satoko Okayama and Kenzaburo Tani performed the experiments. Daisuke Sugiyama designed the experiments and wrote the manuscript.

Conflict of Interest All disclosures will be published when the manuscript is accepted.

References

1. Takahashi, K., & Yamanaka, S. (2006). Induction of pluripotent stem cells from mouse embryonic and adult fibroblast cultures by defined factors. *Cell, 126*, 663–676.
2. Wernig, M., Meissner, A., Foreman, R., et al. (2007). In vitro reprogramming of fibroblasts into a pluripotent ES-cell-like state. *Nature, 448*, 318–324.

3. Okita, K., Ichisaka, T., & Yamanaka, S. (2007). Generation of germline-competent induced pluripotent stem cells. *Nature, 448*, 313–317.
4. Yu, J., Vodyanik, M. A., Smuga-Otto, K., et al. (2007). Induced pluripotent stem cell lines derived from human somatic cells. *Science, 318*, 1917–1920.
5. Nelson, T. J., Martinez-Fernandez, A., Yamada, S., Mael, A. A., Terzic, A., & Ikeda, Y. (2009). Induced pluripotent reprogramming from promiscuous human stemness related factors. *Clinical and Translational Science, 2*, 118–126.
6. Nakagawa, M., Koyanagi, M., Tanabe, K., et al. (2008). Generation of induced pluripotent stem cells without Myc from mouse and human fibroblasts. *Nature Biotechnology, 26*, 101–106.
7. Stadtfeld, M., Brennand, K., & Hochedlinger, K. (2008). Reprogramming of pancreatic beta cells into induced pluripotent stem cells. *Current Biology, 18*, 890–894.
8. Okita, K., Nakagawa, M., Hyenjong, H., Ichisaka, T., & Yamanaka, S. (2008). Generation of mouse induced pluripotent stem cells without viral vectors. *Science, 322*, 949–953.
9. Aoi, T., Yae, K., Nakagawa, M., et al. (2008). Generation of pluripotent stem cells from adult mouse liver and stomach cells. *Science, 321*, 699–702.
10. Hanna, J., Markoulaki, S., Schorderet, P., et al. (2008). Direct reprogramming of terminally differentiated mature B lymphocytes to pluripotency. *Cell, 133*, 250–264.
11. Takenaka, C., Nishishita, N., Takada, N., Jakt, L. M., & Kawamata, S. (2010). Effective generation of iPS cells from CD34+ cord blood cells by inhibition of p53. *Experimental Hematology, 38*, 154–162.
12. Kulkeaw, K., Horio, Y., Mizuochi, C., Ogawa, M., & Sugiyama, D. (2010). Variation in hematopoietic potential of induced pluripotent stem cell lines. *Stem Cell Reviews, 6*, 381–389.
13. Huber, T. L., Kouskoff, V., Fehling, H. J., Palis, J., & Keller, G. (2004). Haemangioblast commitment is initiated in the primitive streak of the mouse embryo. *Nature, 432*, 625–630.
14. Lengerke, C., Grauer, M., Niebuhr, N. I., et al. (2009). Hematopoietic development from human induced pluripotent stem cells. *Annals of the New York Academy of Sciences, 1176*, 219–227.
15. Era, T., Izumi, N., Hayashi, M., Tada, S., & Nishikawa, S. (2008). Multiple mesoderm subsets give rise to endothelial cells, whereas hematopoietic cells are differentiated only from a restricted subset in embryonic stem cell differentiation culture. *Stem Cells, 26*, 401–411.
16. Kataoka, H., Takakura, N., Nishikawa, S., et al. (1997). Expressions of PDGF receptor alpha, c-Kit and Flk1 genes clustering in mouse chromosome 5 define distinct subsets of nascent mesodermal cells. *Development, Growth & Differentiation, 39*, 729–740.
17. Sakurai, H., Era, T., Jakt, L. M., Okada, M., Nakai, S., & Nishikawa, S. (2006). In vitro modeling of paraxial and lateral mesoderm differentiation reveals early reversibility. *Stem Cells, 24*, 575–586.
18. Choi, K., Kennedy, M., Kazarov, A., Papadimitriou, J. C., & Keller, G. (1998). A common precursor for hematopoietic and endothelial cells. *Development, 125*, 725–732.
19. Fehling, H. J., Lacaud, G., Kubo, A., et al. (2003). Tracking mesoderm induction and its specification to the hemangioblast during embryonic stem cell differentiation. *Development, 130*, 4217–4227.
20. Chapman, D. L., Agulnik, I., Hancock, S., Silver, L. M., & Papaioannou, V. E. (1996). Tbx6, a mouse T-Box gene implicated in paraxial mesoderm formation at gastrulation. *Developmental Biology, 180*, 534–542.
21. Wilkinson, D. G., Bhatt, S., & Herrmann, B. G. (1990). Expression pattern of the mouse T gene and its role in mesoderm formation. *Nature, 343*, 657–659.
22. Whitelaw, E., Tsai, S. F., Hogben, P., & Orkin, S. H. (1990). Regulated expression of globin chains and the erythroid transcription factor GATA-1 during erythropoiesis in the developing mouse. *Molecular and Cellular Biology, 10*, 6596–6606.
23. Miller, I. J., & Bieker, J. J. (1993). A novel, erythroid cell-specific murine transcription factor that binds to the CACCC element and is related to the Kruppel family of nuclear proteins. *Molecular and Cellular Biology, 13*, 2776–2786.
24. Varlakhanova, N. V., Cotterman, R. F., & deVries, W. N. (2010). Myc maintains embryonic stem cell pluripotency and self-renewal. *Differentiation, 80*, 9–19.
25. Smith, K. N., Singh, A. M., & Dalton, S. (2010). Myc represses primitive endoderm differentiation in pluripotent stem cells. *Cell Stem Cell, 7*, 343–54.
26. Martinez-Fernandez, A., Nelson, T. J., Ikeda, Y., & Terzic, A. (2010). c-MYC independent nuclear reprogramming favors cardiogenic potential of induced pluripotent stem cells. *Journal of Cardiovascular Translational Research, 3*, 13–23.
27. Polo, J. M., Liu, S., & Figueroa, M. E. (2010). Cell type of origin influences the molecular and functional properties of mouse induced pluripotent stem cells. *Nature Biotechnology, 28*, 848–55.
28. Loh, Y. H., Agarwal, S., & Park, I. H. (2009). Generation of induced pluripotent stem cells from human blood. *Blood, 113*, 5476–9.

Biochemical and Biophysical Research Communications 410 (2011) 301–306

Contents lists available at ScienceDirect

Biochemical and Biophysical Research Communications

journal homepage: www.elsevier.com/locate/ybbrc

Hepatoblasts comprise a niche for fetal liver erythropoiesis through cytokine production

Daisuke Sugiyama *, Kasem Kulkeaw, Chiyo Mizuochi, Yuka Horio, Satoko Okayama

Division of Hematopoietic Stem Cells, Advanced Medical Initiatives, Department of Advanced Medical Initiatives, Kyushu University Faculty of Medical Sciences, Fukuoka 812-8582, Japan

ARTICLE INFO

Article history:
Received 18 May 2011
Available online 30 May 2011

Keywords:
Hepatoblasts
Erythropoiesis
Fetal liver

ABSTRACT

In mammals, definitive erythropoiesis first occurs in fetal liver (FL), although little is known about how the process is regulated. FL consists of hepatoblasts, sinusoid endothelial cells and hematopoietic cells. To determine niche cells for fetal liver erythropoiesis, we isolated each FL component by flow cytometry. mRNA analysis suggested that Dlk-1-expressing hepatoblasts primarily expressed *EPO* and *SCF*, genes encoding erythropoietic cytokines. EPO protein was detected predominantly in hepatoblasts, as assessed by ELISA and immunohistochemistry, and was not detected in sinusoid endothelial cells and hematopoietic cells. To characterize hepatoblast function in FL, we analyzed *Map2k4*$^{-/-}$ mouse embryos, which lack hepatoblasts, and observed down-regulation of *EPO* and *SCF* expression in FL relative to wild-type mice. Our observations demonstrate that hepatoblasts comprise a niche for erythropoiesis through cytokine secretion.

1. Introduction

Hematopoiesis is the process by which pluripotent hematopoietic stem cells (HSCs) are generated, differentiate into specific progenitors, and ultimately mature into numerous blood cell types, including erythrocytes, megakaryocytes, lymphocytes, neutrophils, and macrophages [1]. In the mouse embryo, HSCs and hematopoietic progenitors (HPCs) are generated in the aortic region, known as the para-aortic Splanchnopleura (p-Sp)/Aorta–Gonad–Mesonephros (AGM) region, the yolk sac (YS), and the placenta [2–9]. In mid-gestation, hematopoiesis, particularly erythropoiesis, occurs in fetal liver (FL) [2,9,10]. Erythropoiesis has been classically described as occurring in two waves: first primitive and then definitive erythropoiesis [4]. Primitive erythropoiesis supports a transient wave of embryonic erythropoiesis in the yolk sac, while definitive erythropoiesis contributes to adult-type erythropoiesis. In mammals, definitive erythropoiesis occurs first in FL and then shifts to adult bone marrow (BM) shortly before birth [11]. There are greater numbers of erythroid progenitors, such as burst-forming unit-erythroids (BFU-E) and colony-forming unit-erythroids (CFU-E), in FL than in BM [12]. In addition, in mice, the number of mature erythroid cells in circulation dramatically increases from 12.5 to 16.5 day post-coitum (dpc), suggesting that massive expansion of both erythroid progenitors and terminally differentiated erythroid cells occurs in FL [13]. Erythropoietin (EPO) is a cytokine that regulates erythroid cell differentiation, maturation, proliferation and survival, and is primarily produced by adult kidney cells, where production is up-regulated by hypoxia [14]. Terminal proliferation and differentiation of CFU-E is stimulated by EPO, whereas BFU-E, which are more immature than CFU-E, respond to stem cell factor (SCF), insulin-like growth factor (IGF)-1, corticosteroids, interleukin (IL)-3 and IL-6, in addition to EPO [15]. Although FL is the most active organ for erythropoiesis, little is known about how erythropoiesis is regulated in that tissue.

Here, in order to identify niche cells for erythropoiesis, we used flow cytometry based on surface molecule expression to separate cells in early FL into hepatoblasts (HBs), sinusoid endothelial cells (SECs) and hematopoietic cells (HCs), and then evaluated cytokine expression in each fraction.

2. Materials and methods

2.1. Animals

ICR and C57BL/6J mice were purchased from Nihon SLC (Hamamatsu, Japan) and Kyudo (Tosu, Japan), respectively. *Map2k4*$^{+/-}$ mice were provided by RIKEN BioResource Center (Tsukuba, Japan). Noon of the day of the plug was defined as 0.5 day post-coitum (dpc). Embryos at 12.5 and 14.5 dpc were dissected in PBS under a stereomicroscope. Animals were handled according to Guidelines for Laboratory Animals of Kyushu University.

* Corresponding author. Address: Division of Hematopoietic Stem Cells, Advanced Medical Initiatives, Department of Advanced Medical Initiatives, Kyushu University Faculty of Medical Sciences, Station for Collaborative Research1 4F, 3-1-1 Maidashi, Higashi-Ku, Fukuoka 812-8582, Japan. Fax: +81 92 642 6146.
E-mail address: ds-mons@yb3.so-net.ne.jp (D. Sugiyama).

0006-291X/$ - see front matter © 2011 Elsevier Inc. All rights reserved.
doi:10.1016/j.bbrc.2011.05.137

2.2. Flow cytometry

For hepatoblasts and sinusoid endothelial cells, fetal livers at 12.5 and 14.5 dpc were digested in 1 mg/mL collagenase (Washington Biochem Co., Freehold, New Jersey) in alpha-MEM containing 20% FBS, filtered through 40-μm nylon mesh, and washed once with PBS. Cells were stained with a FITC-conjugated anti-mouse Dlk-1 Ab (MBL, Nagoya, Japan), a PE-conjugated anti-mouse Lyve-1 Ab (MBL), an APC-conjugated anti-mouse CD31 Ab (Bioleged, San Diego, CA), a PE-Cy7-conjugated anti-mouse CD45 Ab (eBioscience, San Diego, CA), and a PE-Cy7-conjugated anti-mouse Ter119 Ab (eBioscience).

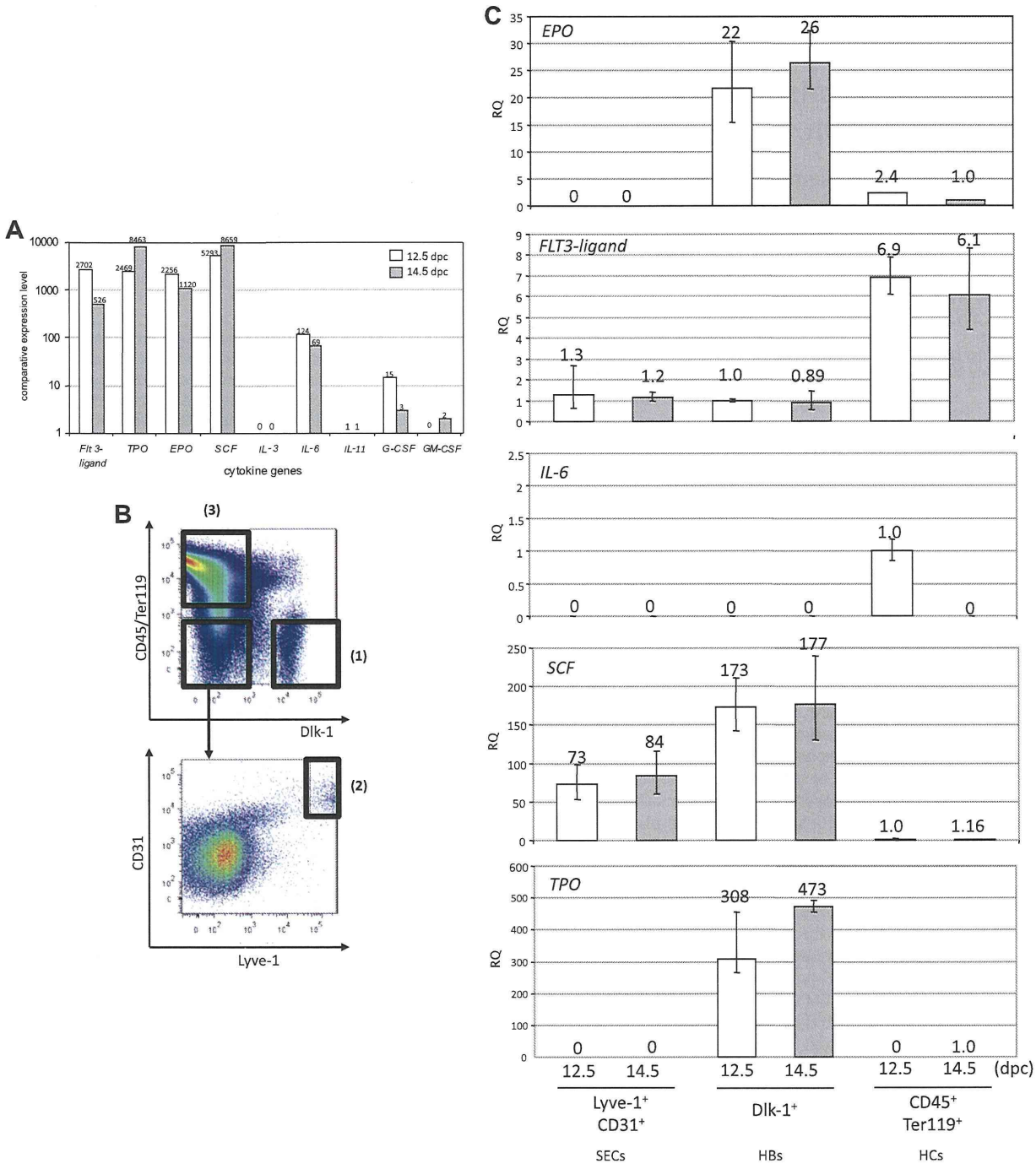

Fig. 1. Cytokine gene expression in fetal liver. (A) *FMS-like tyrosine kinase 3 ligand (Flt3l), thrombopoietin (TPO), eryrhropoietin (EPO), stem cell factor (SCF), interleukin-3 (IL-3), interleukin-6 (IL-6), interleukin-11 (IL-11), granulocyte-colony stimulating factor (G-CSF) and granulocyte/macrophage-colony stimulating factor (GM-CSF)* mRNAs were examined in FL samples at 12.5 and 14.5 dpc by real-time PCR. Note high expression of *Flt3l, TPO, EPO* and *IL-6* in FL. (B) A single cell suspension was obtained from FL at 12.5 dpc and expression of CD45/Ter119, Dlk-1, Lyve-1 and CD31 was analyzed by flow cytometry. (1) CD45−/Ter119−/Dlk-1+ defines HBs; (2) CD45−/Ter119−/Lyve-1+/CD31+ defines SECs; and (3) CD45+/Ter119+ defines HCs. (C) Expression of *Flt3l, TPO, EPO* and *IL-6* was examined by real-time PCR in HBs, SECs and HCs sorted by flow cytometry, according to gates defined in Fig. 1B. EPO and TPO expression was high in HBs at both 12.5 dpc and 14.5 dpc. SCF expression was higher in HBs than in SECs. Expression of *Flt3l* was high in HCs. Expression of *IL-6* was detected only in HCs.

2.3. Real time-PCR

RNA was extracted from sorted and fetal liver samples using a RiboPure™ kit (Life Technologies, Carlsbad, CA) and mRNA was reverse transcribed using a High-Capacity RNA-to-cDNA kit (Life Technologies). cDNA synthesis quality was evaluated by amplifying mouse β-*actin* by PCR. Thirty thermal cycles were employed as follows: denaturation at 95 °C for 10 s, annealing at 60 °C for 20 s, and extension at 72 °C for 20 s. Gene expression levels were measured by real time-PCR with TaqMan® Gene Expression Master Mix and StepOnePlus™ real time PCR (Life Technologies). All probes (*Flt3-L, TPO, EPO, SCF, IL-3, IL-6, IL-11, G-CSF* and *GM-CSF*) were from TaqMan® Gene Expression Assays (Life Technologies). All samples were assayed in triplicate wells. mRNA levels were normalized to β-*actin* and the relative quantity (RQ) of expression was compared with a reference sample.

2.4. Enzyme-Linked Immunosorbent assay (ELISA)

Lysates of sorted cells were obtained using a cell lysis buffer (M-Per® Mammalian Protein Extraction Reagent, Thermo Fisher Scientific, Waltham, MA) containing protease inhibitors (Protease Inhibitor Cocktail, Sigma–Aldrich, St. Louis, MO). The sample was centrifuged at 14000*g* at 4 °C for 15 min. Supernatants containing soluble protein were collected and protein concentration was estimated by measuring absorbance at 280 nm (NANODROP 2000C, Thermo Fisher Scientific). SCF and EPO in sorted cells were assayed using an ELISA kit (Mouse SCF Immunoassay and Mouse EPO Immunoassay, R&D systems) according to the manufacturer's instructions. Experiments were performed in duplicate. The OD was measured using a Thermo Multiskan FC plate reader (Thermo Fisher Scientific).

2.5. Immunohistochemistry

Dissected ICR mouse embryos were fixed in 2% paraformaldehyde in PBS overnight at 4 °C and washed in PBS three times. After 27% sucrose infusion, embryos were embedded in OCT compound (Sakura Finetek, Tokyo, Japan) and frozen in liquid nitrogen (vapor phase). Frozen embryos were sectioned at 20 μm, transferred onto glass slides (Matsunami, Osaka, Japan), and dried. After blocking in 1% BSA in PBS, sections were incubated with primary antibodies overnight at 4 °C. Anti-mouse Dlk-1 Ab (MBL), anti-mouse Lyve-1 Ab (MBL), anti-mouse c-Kit Ab (R&D Systems), anti-mouse SCF Ab (Santa Cruz Biotechnology, Santa Cruz, CA), anti-mouse EPO Ab (Santa Cruz Biotechnology, Santa Cruz, CA) and anti-mouse Ki-67 Ab (Dako Corporation, Carpinteria, CA) served as primary antibodies. After washing in PBS three times, sections stained with Dlk-1, Lyve-1, c-Kit or Ki-67 antibodies were incubated with secondary antibodies and TOTO-3 (Life Technologies) for nuclear staining. In samples stained with SCF or EPO antibodies, the TSA Biotin System (PerkinElmer, Covina, CA) was used to amplify the signal. Donkey anti-rabbit IgG-Alexa555, Donkey anti-goat IgG-Alexa488, Donkey anti-rat IgG-Alexa488 and Alexa546 and

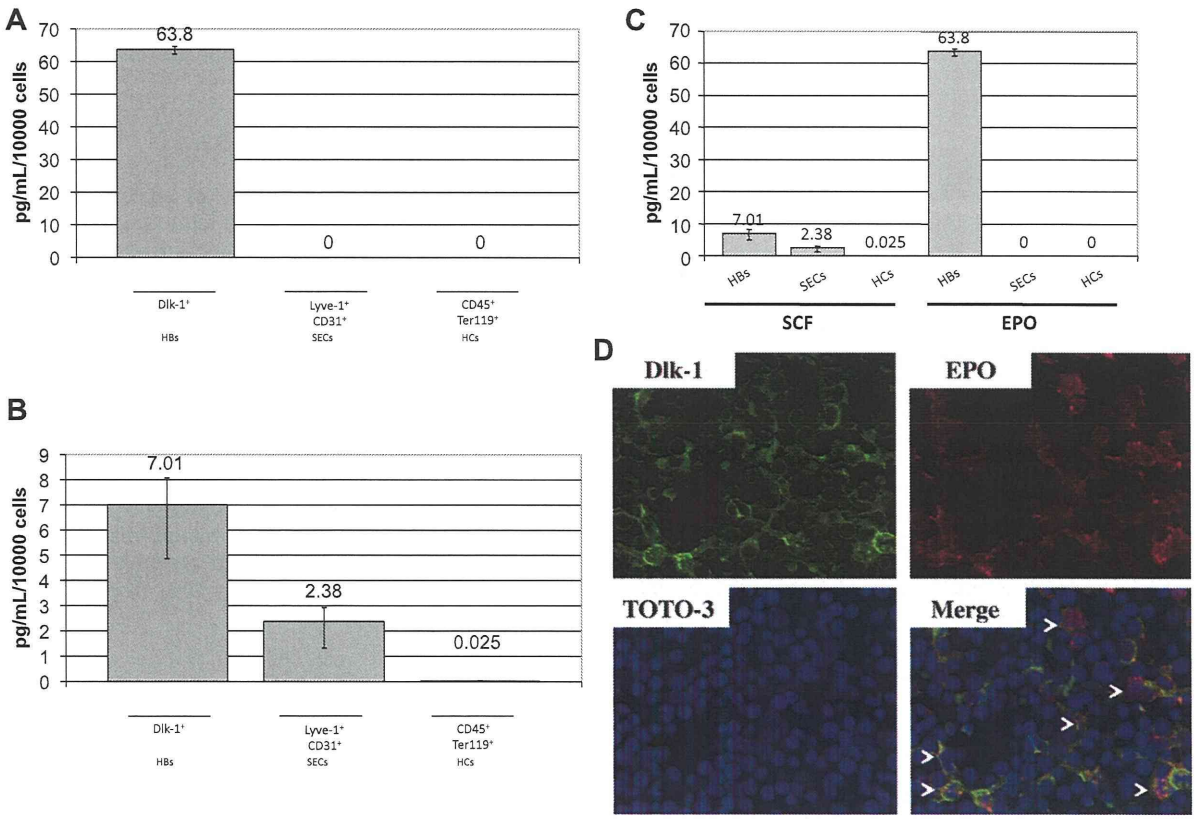

Fig. 2. Expression of EPO and SCF protein in fetal liver. (A) EPO protein in sorted cells was assayed by ELISA. EPO was detected in HBs (63.8 pg/mL/10,000 cells) but not in SECs and HCs at 12.5 dpc. (B) SCF protein in sorted cells was assayed by ELISA. SCF was detected in HBs (7.01 pg/mL/10,000 cells), SECs (2.38 pg/mL/10,000 cells) and HCs (0.025 pg/mL/10,000 cells) at 12.5 dpc. (C) The data from Fig. 2A with 2B were combined to compare EPO and SFC protein expression in each fraction sorted from fetal liver. EPO protein expression was highest in HBs. (D–F) Liver sections were prepared from ICR mouse embryos at 12.5 dpc and stained with Dlk-1 (green), EPO (red) and TOTO-3 (blue) (D); Lyve-1 (green), SCF (red) and TOTO-3 (blue) (E); and Dlk-1 (green), SCF (red) and TOTO-3 (blue) (F). Arrowheads show co-localization of the antigens, respectively. Samples were observed under confocal microscopy. EPO was primarily expressed in HBs expressing Dlk-1, whereas SCF was more widely expressed in FL. Original magnification is 40× (D–F).

Streptavidin Alexa546 (all from Life Technologies) served as secondary antibodies. Coverslips were mounted using fluorescent mounting medium (Dako Corporation, Carpinteria, CA). Slides were observed using a FV-1000 confocal microscope (Olympus, Tokyo, Japan).

2.6. Single cell preparation and cell counting

To prepare single cell suspensions of HCs from *Map2k4*$^{-/-}$ and wild-type FL at 12.5 dpc, dissected FL was crushed on the 40 μm nylon cell strainer (BD Falcon, Bedford, MA) with the inner of 2.5 mL syringe. Cells were washed in PBS and collected into the tube. The number of living cells was counted after Trypan Blue staining.

3. Results

3.1. Cytokine expression in hepatoblasts

We examined expression of several cytokine genes in FL tissue samples at 12.5 and 14.5 dpc using real-time PCR. Significant expression of FMS-like tyrosine kinase 3 ligand (*Flt3l*), thrombopoietin (*TPO*), erythropoietin (*EPO*) and interleukin-6 (*IL-6*) was seen in FL (Fig. 1A). Dlk-1 (Delta-like 1 homolog) is a marker of hepatoblasts (HBs) in FL [16], while Lyve-1 (lymphatic vessel endothelial hyaluronan receptor 1) marks sinusoid endothelial cells (SECs) [17]. As shown in Fig. 1B, fractions of HBs, SECs and hematopoietic cells (HCs) were isolated from mouse FL at both 12.5 and 14.5 dpc by flow cytometry based on expression of the following surface markers: (1) HBs, CD45−/Ter119−/Dlk-1+; (2) SECs, CD45−/Ter119−/Lyve-1+/CD31+; and (3) HCs, CD45+/Ter119+. To determine which component contributes to cytokine production, we used real-time PCR to examine *EPO*, *Flt3l*, *IL-6*, *SCF* and *TPO* expression in isolated HBs, SECs and HCs (Fig. 1C). *EPO* and *TPO* were expressed predominantly in HBs both at 12.5 and 14.5 dpc, suggesting that erythropoiesis and megakaryopoiesis are activated by HBs in FL. Levels of *SCF* mRNA were higher in HBs than in SECs. Expression of *Flt3l* and *IL-6* was predominantly detected in HCs, suggesting that HSCs and HPCs expand via an autocrine mechanism. To investigate expression of the cytokine proteins EPO and SCF, we undertook Enzyme-Linked ImmunoSorbent assay (ELISA) and found that EPO protein was predominantly detected in HBs (63.8 pg/mL/10,000 cells) but was not detected in SECs and HCs (Fig. 2A). SCF protein, however, was detected in all fractions (Fig. 2B). In agreement with *SCF* mRNA expression, HBs expressed SCF protein at a higher level (7.01 pg/mL/10,000 cells) than did SECs (2.38 pg/mL/10,000 cells) or HCs (0.025 pg/mL/10,000 cells). When we compared expression levels of EPO and SCF proteins in each fraction, EPO expression was highest in HBs, suggesting that HBs secrete EPO to regulate FL erythropoiesis (Fig. 2C). To confirm EPO and SCF protein localization in FL, we performed immunohistochemistry and found that EPO protein was expressed primarily in Dlk-1-expressing HBs (Fig. 2D), in agreement with ELISA analysis. Staining of FL with anti-SCF antibody revealed SCF protein in both SECs expressing Lyve-1 and HBs expressing Dlk-1 (Fig. 2E and F).

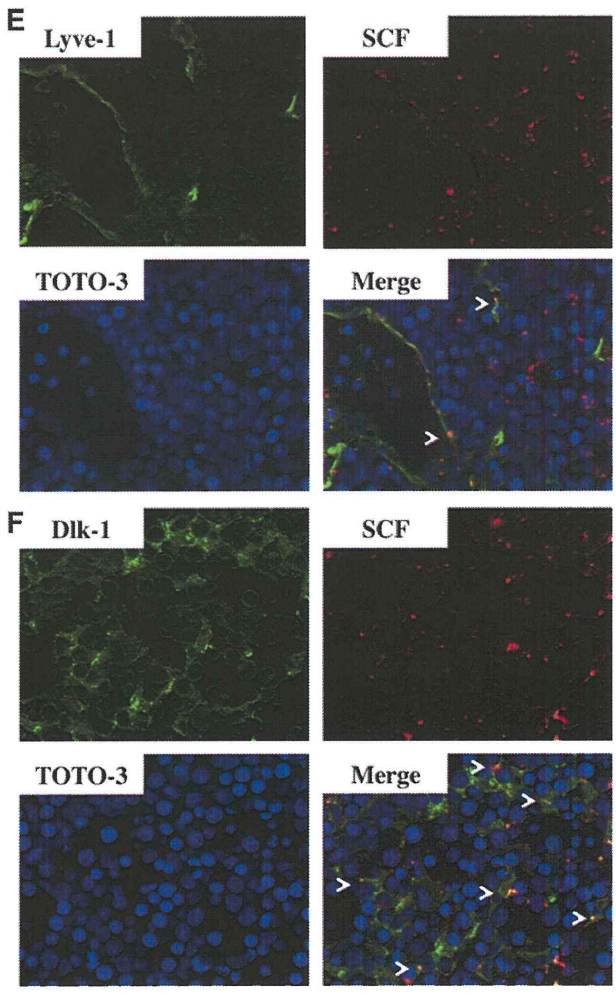

Fig. 2 (*continued*)

3.2. Fetal liver of *Map2k4*$^{-/-}$ mouse embryos

To characterize HB function in FL, we analyzed *Map2k4* (*mitogen-activated protein kinase kinase 4*, formerly known as *Sek1* and *MKK4*)$^{-/-}$ mouse embryos, which lack FL HBs [18–20]. Real-time PCR analysis of whole FL from mutant and wild-type embryos showed that among cytokine-encoding genes, *EPO* and *SCF* mRNAs were down-regulated in the mutant mice, implying an impairment in hematopoiesis, particularly erythropoiesis, in *Map2k4* mutant mice (Fig. 3A). To evaluate potential alterations in hematopoiesis, we performed immunohistochemistry and found that the number of c-Kit expressing cells which represent HSCs and HPCs in the FL at this stage, decreased in a FL field from *Map2k4*$^{-/-}$ mouse embryo relative to wild-type embryo (Fig. 3B; green) [23]. In addition, the number of cells expressing Ki-67, a marker of cell proliferation, decreased in a FL field from *Map2k4*$^{-/-}$ mouse embryos compared to wild-type embryos (Fig. 3B; red). In agreement with the Ki-67 staining, there were fewer FL cells seen in *Map2k4*$^{-/-}$ versus wild-type embryos (Fig. 3C).

4. Discussion

In FL, HSCs differentiate into mature HCs, particularly erythroid cells [9,10]. SCF and EPO are representative cytokines that regulate erythropoiesis [14,15]. Expression levels of *SCF* and *EPO* genes were higher in whole FL tissue than in adult BM and kidney, suggesting that FL primarily functions in erythropoiesis [24]. Recently, using a competitive repopulating assay, Chou and Lodish reported that FL stromal cells expressing both SCF and Dlk-1 support HSC maintenance [25]. However, it remained unclear which cells secreted EPO in FL. HBs are regarded as common progenitors of hepatocytes and biliary epithelial cells and thought to support liver

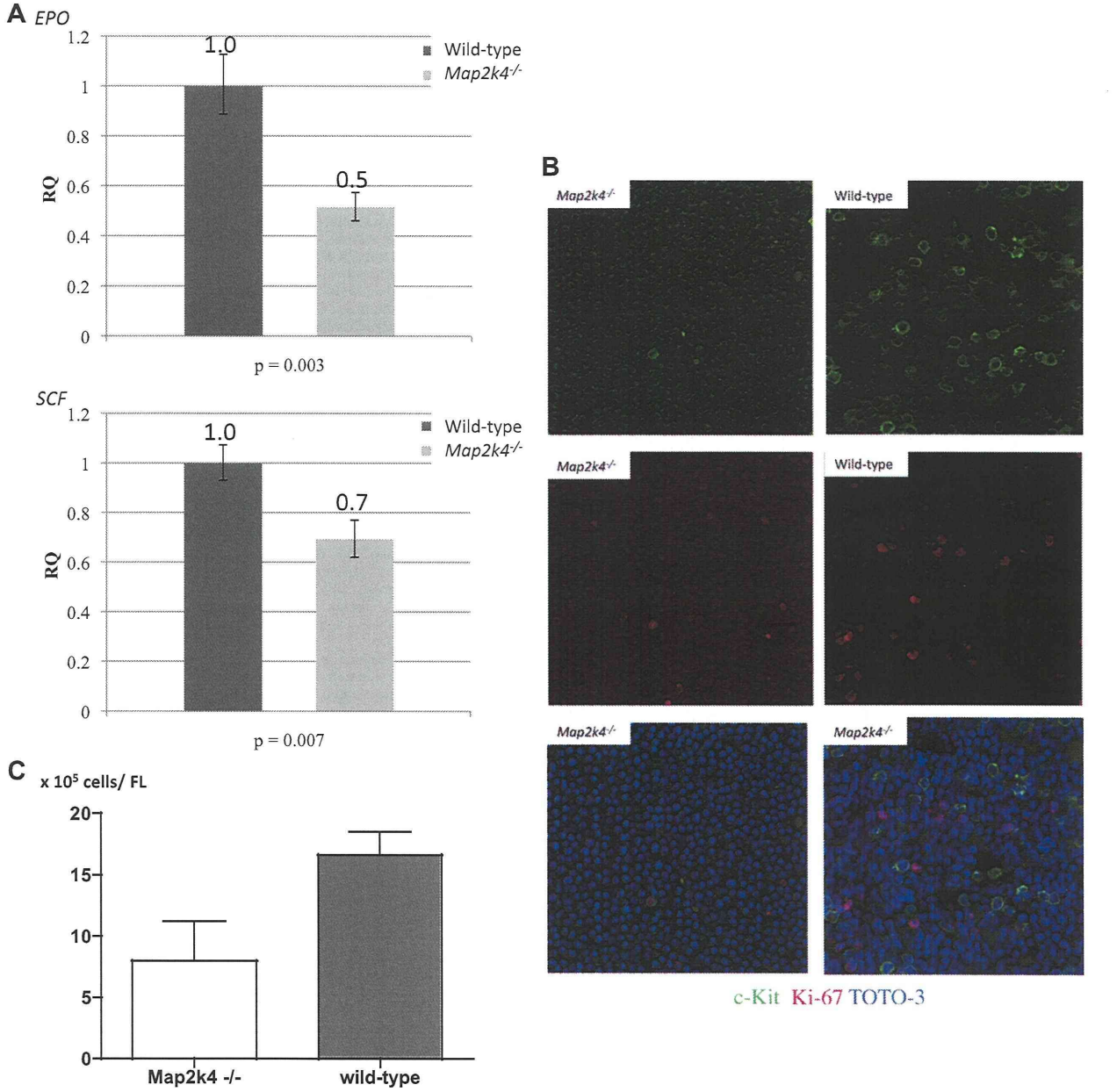

Fig. 3. Phenotypic analysis of FL in *Map2k4*$^{-/-}$ mouse embryos. (A) Expression of *EPO* and *SCF* was examined by real-time PCR in *Map2k4*$^{-/-}$ fetal liver (FL). Expression levels of both *EPO* and *SCF* were down-regulated in *Map2k4*$^{-/-}$ FL relative to wild-type FL. (B) Liver sections were made from both *Map2k4*$^{-/-}$ and wild-type mouse embryos at 12.5 dpc, stained with c-Kit (green), Ki-67 (red) and TOTO-3 (blue), and observed under confocal microscopy. The number of Ki-67 positive cells in a field decreased in *Map2k4*$^{-/-}$ FL compared to wild-type FL. Original magnification is 40×. (C) Single cell suspensions were obtained from *Map2k4*$^{-/-}$ and wild-type FL at 12.5 dpc and the number of living cells was counted after Trypan Blue staining. Significant decreases in the number of *Map2k4*$^{-/-}$ FL cells were observed compared to wild-type FL cells. (For interpretation of the references to color in this figure legend, the reader is referred to the web version of this article.)

construction through formation of a mesh-like structure [16,26]. Our results are strongly indicative of an additional role of HBs in producing erythropoietic cytokines SCF and EPO. Although gene expression of *IL-6* was observed in FL at 12.5 dpc, that was not detected in cell fractions of HBs, SECs and HCs (Fig. 1). As shown in Fig. 1B, we could observe unclassified cell fraction (CD45−/Ter119−/Dlk-1−/Lyve-1−/CD31−), based on surface marker expression, implying that this unclassified cell fraction may express *IL-6* gene. It will be further necessary to clarify roles of the unclassified cells in FL hematopoiesis in the future.

The c-Jun NH_2-terminal protein kinases (JNKs) are members of the mitogen-activated protein kinase (MAPK) family. Map2k4 is a MAPK kinase that directly activates JNKs in response to extracellular and intracellular stresses, and its deficiency leads to abnormal hepatogenesis, resulting in loss of HBs [20,27–29]. In situ hybridization shows that expression of *Map2k4* transcripts is detected in FL by 12.5 dpc and then up-regulated until 16.5 dpc, at which time expression is down-regulated [30]. When *Map2k4*$^{-/-}$ FL cells were transplanted into *rag1*$^{-/-}$ adult mice, both B cells and T cells were generated, demonstrating that *Map2k4*$^{-/-}$ FL cells contain HSCs and/or HPCs [28]. In addition, normal hematopoiesis reportedly occurs in the *Map2k4*$^{-/-}$ YS at both 9.5 and 10.5 dpcs, based on erythroid, myeloid and mixed colony formation [28]. Taken together, hematopoietic potential of *Map2k4*$^{-/-}$ FL looked normal

compared to wild-type mice. Therefore, the decrease of hematopoietic cells were likely due to lack of HBs, but not due to alteration of hematopoietic potential in *Map2k4*$^{-/-}$ FL. Recently, Hikita et al. reported a novel mouse model lacking both HBs and hepatocytes using an *Alb* Cre driver [31]. This mutant mouse, generated by crossing *Alb Cre* mice with both *bcl-xl*$^{flox/flox}$ mice and *mcl-1*$^{flox/flox}$ mice, showed a decreased number of hepatocytes at 18.5 dpc. Future studies will be required to address the function of HBs and hepatocytes in FL erythropoiesis using this model.

5. Conclusion

Hepatoblasts comprise a niche for erythropoiesis through cytokine secretion.

Authorship contributions

D. Sugiyama designed the research, performed research, analyzed data and wrote the paper. K. Kulkeaw performed research and analyzed data. C. Mizuochi, Y. Horio and S. Okayama performed research.

Conflict of interest

The authors have no conflict of interest to declare.

Acknowledgments

The authors acknowledge grant support from the Special Coordination Funds for Promoting Science and Technology, a Grant-in-Aid for Young Scientists (B) from The Ministry of Education, Culture, Sports, Science and Technology, Grant-in-Aid by Ministry of Health, Labor and Welfare, Bilateral Joint Projects for Japan Society for the Promotion of Science, the Ajinomoto Scholarship Foundation and the Tokyo Biochemical Research Foundation. We thank the Research Support Center, the Graduate School of Medical Sciences, Kyushu University, for technical support, Drs. K. Akashi and K. Tani for helpful discussion, Dr. T. Inoue for technical support, and Dr. Elise Lamar for critical reading of the manuscript.

References

[1] I.L. Weissman, Stem cells: units of development, units of regeneration, and units in evolution, Cell 100 (2000) 157–168.
[2] E. Dzierzak, A. Medvinsky, M. de Bruijn, Qualitative and quantitative aspects of hematopoietic cell development in the mammalian embryo, Immunol. Today 19 (1998) 228–236.
[3] S. Matsuoka, K. Tsuji, H. Hisakawa, et al., Generation of definitive hematopoietic stem cells from murine early yolk sac and paraaortic splanchnopleures by aorta–gonad–mesonephros region-derived stromal cells, Blood 98 (2001) 6–12.
[4] D. Sugiyama, K. Tsuji, Definitive hematopoiesis from endothelial cells in the mouse embryo; a simple guide, Trends Cardiovasc. Med. 16 (2006) 45–49.
[5] B.M. Zeigler, D. Sugiyama, M. Chen, Y. Guo, K.M. Downs, N.A. Speck, The allantois and chorion when isolated before circulation or chorio-allantoic fusion, have hematopoietic potential, Development 133 (2006) 4183–4192.
[6] I.M. Samokhvalov, N.I. Samokhvalova, S. Nishikawa, Cell tracing shows the contribution of the yolk sac to adult haematopoiesis, Nature 446 (2007) 1056–1061.
[7] K.E. Rhodes, C. Gekas, Y. Wang, et al., The emergence of hematopoietic stem cells is initiated in the placental vasculature in the absence of circulation, Cell Stem Cell 2 (2008) 252–263.
[8] T. Sasaki, C. Mizuochi, Y. Horio, K. Nakao, K. Akashi, D. Sugiyama, Regulation of hematopoietic cell clusters in the placental niche through SCF/Kit signaling in embryonic mouse, Development 137 (2010) 3941–3952.
[9] G.R. Johnson, R.O. Jones, Differentiation of the mammalian hepatic primordium in vitro. I Morphogenesis and the onset of haematopoiesis, J. Embryol. Exp. Morphol. 30 (1973) 83–96.
[10] G.R. Johnson, M.A. Moore, Role of stem cell migration in the initiation of mouse foetal liver haemopoiesis, Nature 258 (1975) 726–728.
[11] J. Palis, S. Robertson, M. Kennedy, C. Wall, G. Keller, Development of erythroid and myeloid progenitors in the yolk sac and embryo proper of the mouse, Development 126 (1999) 5073–5084.
[12] H. Kurata, G.C. Mancini, G. Alespeiti, A.R. Miqliaccio, G. Miqliaccio, Stem cell factor induces proliferation and differentiation of fetal progenitor cell in the mouse, Br. J. Haematol. 101 (1998) 676–687.
[13] P.D. Kingsley, J. Malik, K.A. Fantauzzo, J. Palis, Yolk sac-derived primitive erythroblasts enucleate during mammalian embryogenesis, Blood 104 (2004) 19–25.
[14] H. Lodish, J. Flygare, S. Chou, From stem regulation of red cell production at multiple levels by mutiple hormones, IUBMB Life 62 (2010) 492–496.
[15] G. Molineux, M.A. Foote, S. Elliott, Erythropoietins and Erythropoiesis, Birkhauser, Basel, Switzerland, 2009.
[16] N. Tanimizu, M. Nishikawa, H. Saito, T. Tsujimura, A. Miyajima, Isolation of hepatoblasts based on the expression of Dlk/Pref-1, J. Cell Sci. 116 (2003) 1775–1786.
[17] C. Mouta Carreira, S.M. Nasser, E. di Toamaso, T.P. Padera, Y. Boucher, S.I. Tomarev, R.K. Jain, LYVE-1 is not restricted to the lymph vessels: expression in normal liver blood sinusoids and down-regulation in human liver cancer and cirrhosis, Cancer Res. 61 (2001) 8079–8084.
[18] H. Nishina, K.D. Fischer, L. Radvanyi, et al., Stress-signalling kinase Sek1 protects thymocytes from apoptosis mediated by CD95 and CD3, Nature 385 (1997) 350–353.
[19] H. Nishina, M. Bachmann, A.J. Oliveira-dos-Santos, Impaired CD28-mediated interleukin 2 production and proliferation in stress kinase SAPK/ERK1 kinase (SEK1)/mitogen-activated protein kinase kinase 4 (MKK4)-deficient T lymphocytes, J. Exp. Med. 186 (1997) 941–953.
[20] T. Watanabe, K. Nakagawa, S. Ohata, SEK1/MKK4-mediated SAPK/JNK signaling paticipates in embryonic hepatoblast proliferation via a pathway different from NF-κB-induced anti-apoptosis, Dev. Biol. 250 (2002) 332–347.
[23] T. Inoue, D. Sugiyama, R. Kurita, et al., APOA-1 is a novel marker of erythroid cell maturation from hematopoietic stem cells in mice and humans, Stem Cell Rev. 7 (2011) 43–52.
[24] S.J. England, K.E. McGrath, J.M. Frame, J. Palis, Immature erythroblasts with extensive ex vivo self-renewal capacity emerge from the early mammalian fetus, Blood 117 (2010) 2708–2717.
[25] S. Chou, H.F. Lodish, Fetal liver hepatic progenitors are supportive stromal cells for hematopoietic stem cells, Proc. Natl. Acad. Sci. USA 107 (2010) 7799–7804.
[26] K. Sasaki, Y. Sonoda, Histometrical and three-dimensional analyses of liver hematopoiesis in the mouse embryo, Arch. Histol. Cytol. 63 (2000) 137–146.
[27] S. Ganiatsas, L. Kwee, Y. Fujiwara, A. Perkins, T. Ikeda, M.A. Labow, L.I. Zon, SEK1 deficiency reveals mitogen-activated protein kinase cascade crossregulation and leads to abnormal hepatogenesis, Proc. Natl. Acad. Sci. USA 95 (1998) 6881–6886.
[28] H. Nishina, C. Vaz, P. Billia, et al., Defective liver formation and liver cell apoptosis in mice lacking the stress signaling kinase SEK1/MKK4, Development 126 (1999) 505–516.
[29] X. Wang, A. Destrument, C. Tournier, Physiological roles of MKK4 and MKK7: insights from animal models, Biochim. Biophys. Acta 1773 (2007) 1349–1357.
[30] J.K. Lee, W.S. Hwang, Y.D. Lee, P.L. Han, Dynamic expression of SEK1 suggests multiple roles of the gene during embryogenesis and in adult brain of mice, Brain Res. Mol. Brain Res. 66 (1999) 133–140.
[31] H. Hikita, T. Takehara, S. Shimizu, Mcl-1 and Bcl-xL cooperatively maintain integrity of hepatocytes in developing and adult murine liver, Hepatology 50 (2009) 1217–1226.

Genes to Cells

Cold exposure down-regulates zebrafish pigmentation

Kasem Kulkeaw[1], Tohru Ishitani[2], Takaaki Kanemaru[3], Ognen Ivanovski[1,4], Midori Nakagawa[1], Chiyo Mizuochi[1], Yuka Horio[1] and Daisuke Sugiyama[1]*

[1]*Department of Hematopoietic Stem Cells, SSP Stem Cell Unit, Faculty of Medical Sciences, Kyushu University, Fukuoka, Japan*
[2]*Division of Cell Regulation Systems, Department of Post-Genome Science Center, Medical Institute of Bioregulation, Kyushu University, Fukuoka, Japan*
[3]*Morphology Core Unit, Kyushu University Hospital, Fukuoka, Japan*
[4]*University Clinic of Urology, Medical Faculty, University 'Ss Cyril and Methodius,' Skopje, Macedonia*

Vertebrates use adaptive mechanisms when exposed to physiologic stresses. However, the mechanisms of pigmentation regulation in response to physiologic stresses largely remain unclear. To address this issue, we developed a novel pigmentation model in adult zebrafish using coldwater exposure (cold zebrafish). When zebrafish were maintained at 17 °C, the pigmentation of their pigment stripes was reduced compared with zebrafish at 26.5 °C (normal zebrafish). In cold zebrafish, gene expression levels of *tyrosinase* and *dopachrome tautomerase*, which encode enzymes involved in melanogenesis, were down-regulated, suggesting that either down-regulation of melanin synthesis occurred or the number of melanophores decreased. Both regular and electron microscopic observation of zebrafish skin showed that the number of melanophores decreased, whereas aggregation of melanosomes was not changed in cold zebrafish compared with normal zebrafish. Taken together, we here show that cold exposure down-regulated adult zebrafish pigmentation through decreasing the number of melanophores and propose that the cold zebrafish model is a powerful tool for pigmentation research.

Introduction

Cold temperatures affect many physiologic processes in endothermic animals, such as slowing the rate of enzymatic reactions, reducing diffusion and transport of biologic molecules, inducing protein denaturation and misaggregation, slowing gene transcription and translation, disrupting cytoskeletal structure and altering cell membrane permeability (Sonna *et al.* 2002). In contrast to endothermic animals, ectothermic vertebrates, such as fish, possess multiple adaptation mechanisms that allow them to cope with low temperatures, which are as follows: (i) increasing the quantity of enzymes involved in lipid metabolism (Cossins *et al.* 2002), (ii) increasing pump activity, Na^+/K^+-ATPase activity and oxygen consumption in hepatocytes and kidney cells (Schwarzbaum *et al.* 1992a,b) and (iii) up-regulation of genes related to oxidative stress in the skeletal muscle of fish tails (Malek *et al.* 2004). Environmental temperature has been shown to affect the expression levels of the cold-shock proteins (Al-Fageeh & Smales 2006). Low temperature (17 °C) induces the expression of cold-shock domain (CSD) containing C2 (*csdc2*) gene in zebrafish kidney marrow (KM) (Kulkeaw *et al.* 2010). Csdc2 contains an S1-like CSD, which is widely found in the cold-shock proteins of eukaryotes, prokaryotes and archaea. Although the functions of cold-shock proteins remain unclear, they have been shown to bind mRNA to regulate ribosomal translation, mRNA degradation and rate of transcription termination (Al-Fageeh & Smales 2006). Heat-shock proteins are also related to environmental temperature, and expression of *heat shock protein 8* (*hspa8*) decreases in carp when exposed to coldwater temperature (Ali *et al.* 2003).

Studies of zebrafish (*Danio rerio*), a teleost tropical fish, have enhanced our understanding of human and mouse developmental biology. Easy handling of embryos and a short lifespan make zebrafish a suitable

Communicated by: Shigeru Kondo
**Correspondence*: ds-mons@yb3.so-net.ne.jp

DOI: 10.1111/j.1365-2443.2011.01498.x

model for investigations into cellular differentiation, organ development and gene function via genetic manipulation. Zebrafish have also been used in pigmentation research. For example, studies of pigment cell differentiation during zebrafish development have produced several mutant strains: *albino*^{b1}, *golden*^{b2}, *brass*^{b4}, *sparse*^{b5} (Parichy *et al.* 1999), *leopard*^{t1} (Johnson & Weston 1995) and *panther*^{j4blue} (Parichy *et al.* 2000). These studies show that zebrafish is a useful genetic model for studying developmental biology in the field of pigmentation research. In adult zebrafish, pigment is represented as blue and black stripes running along the body length and fins, separated by silver interstripes. The pigment cells (chromatophores) are localized in the hypodermis. Zebrafish have three types of chromatophores: xanthophores (yellow), reflective iridophores and melanophores (black), in order from superficial to deep. Pigmented melanophore formation in adult zebrafish requires the differentiation from melanoblasts, melanin synthesis and translocation of melanin-containing granules, or melanosomes. Melanoblast differentiation has been extensively studied in fin regeneration, and *kita* and *kit ligand a* (*kitlga*) have been identified as crucial proponents (Rawls & Johnson 2000, 2001). *Microphthalmia-associated transcription factor a* (*mitfa*) also plays an important role, by controlling the expression of genes encoding the melanin-synthesizing enzymes, *tyrosinase* (*tyr*) and *dopachrome tautomerase* (*dct*) (White & Zon 2008). It appears that *mitfa* is an early marker of melanoblast differentiation (Lister *et al.* 1999), followed by *kita* (Parichy *et al.* 1999) and *dct* (Kelsh & Eisen 2000). Nonpigmented melanophore then synthesizes melanin, which is stored in melanosomes. The melanosomes are then distributed throughout the cytoplasm of melanophore. It has been reported that melanin-concentrating and melanocyte-stimulating hormones (MCH and MSH, respectively) control melanosome translocation (Logan *et al.* 2006). Both hormones are synthesized in brain and have antagonist effects. MCH is derived from pro-melanin-concentrating hormone (*pmch*) and causes melanosome aggregation, whereas MSH is derived from proopiomelanocortin a (*pomca*) and causes melanosome dispersion. In addition to hormone, aggregation of melanosome of fish melanophores is controlled by sympathetic neurons (Iwashita *et al.* 2006). However, the mechanisms of pigmentation regulation in response to physiologic and environmental stresses remained ill-defined. Alternative pigmentation models are necessary to address this issue. In response, we here show a novel model in zebrafish using coldwater exposure.

Results

Cold exposure down-regulates skin pigmentation in zebrafish

No significant differences were observed between the two groups of zebrafish before cold exposure (results not shown). On day 3 of exposure of one group to cold water, pigmentation of cold zebrafish (17 °C) began to become slightly paler than that of normal zebrafish (26.5 °C) (Fig. 1A). One week after cold exposure, the pigmentation of the cold zebrafish,

Figure 1 Effects of cold exposure on zebrafish pigmentation and growth. (A) Gross appearances of normal and cold zebrafish and their background adaptation. Normal and cold zebrafish were maintained at 26.5 or 17 °C inside of incubator for 3 days (d), 1 week (W) and 2 W. The cold zebrafish appeared pale and depigmented. The degree of depigmentation correlated with the length of cold exposure. In background adaptation (lower panel), zebrafish were maintained at 26.5 °C in the incubator with appropriate light cycle. Two weeks later, the pigmentation of control zebrafish inside of incubator became slightly pale compared with zebrafish maintaining in water tank. (B) Higher magnification of pigment stripes on the body and tail. At 2 W, melanophores of cold zebrafish appeared as spots, whereas melanophores of normal zebrafish spread over larger areas. (C) Melanin content in zebrafish skin. The zebrafish skin was solubilized in Soluene®-350. Melanin was measured by absorption at 500 nm. The bar graphs show the means and standard deviation of optical density per 50 mg of zebrafish skin from three zebrafish per group. The Student's *t*-test was used for statistical analysis. (D) Effects of cold exposure on body weight and size of zebrafish. Cold exposure reduced the growth of zebrafish. Two-month-old zebrafish were maintained in water at 26.5 or 17 °C for 1 W, 2 W and 7 months (Mo). Body weight and length of cold zebrafish were significantly lower than those of normal zebrafish (upper and lower panels, respectively). The bar graphs show the means and standard deviations of body weight and length from 6 to 7 zebrafish per group. Student's *t*-test was used for statistical analysis. (E) Histology of kidney marrow (KM). KM was stained with Toluidine Blue O (left and middle) and observed by transmission electron microscopy (TEM) (right). In 26.5 °C water, there are normal renal tubules (RT) surrounded by hematopoietic cells (HC) (left). Cold zebrafish kept at 17 °C for 7 Mo exhibit abnormal RTs (upper middle). Black pigment-producing cells (lower middle, arrow) were observed only in cold zebrafish. TEM image shows melanin-containing granules in the KM of cold zebrafish (right).

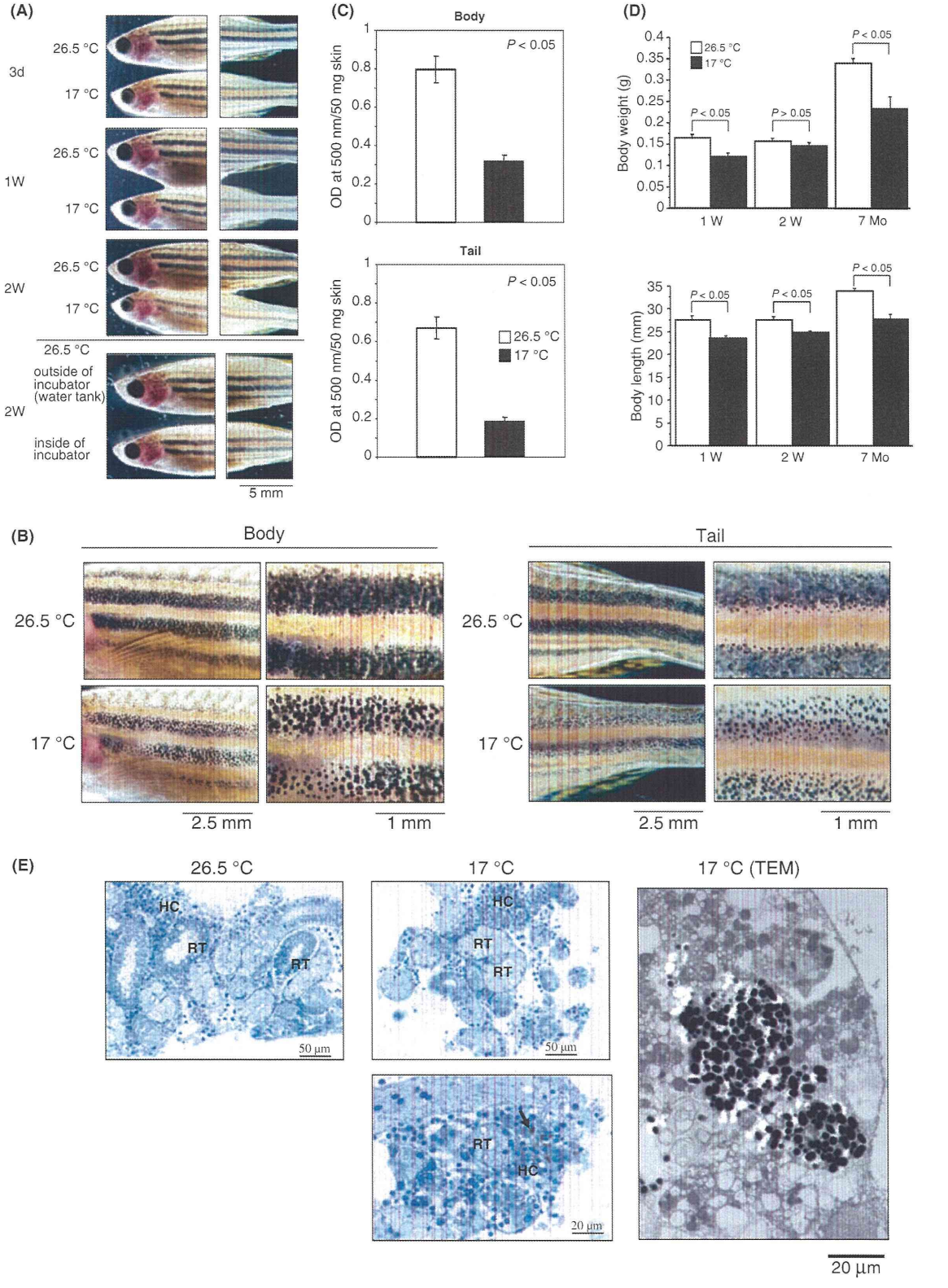

particularly tail, became paler than that of the normal zebrafish. After 2 weeks of cold exposure, the zebrafish pigmentation became even paler (Fig. 1A). High-magnification microscopy of the body flanks and tails showed that the melanophores of cold zebrafish appeared as small spots, as opposed to the larger spots of the normal zebrafish that covered wider area (Fig. 1B). We also assessed the changes in pigmentation before and after cold exposure in individual zebrafish. All cold zebrafish became paler than normal zebrafish (Fig. S1 in Supporting Information). To confirm the down-regulation of pigmentation in cold zebrafish, melanin content was measured by spectrophotometer. Melanin content in the body and tail skin of cold zebrafish was 2.7- and 3.5-fold lower than that of normal zebrafish (Fig. 1C). Moreover, to exclude the possibility that the color adaptation to white background occurred in cold zebrafish, we maintained zebrafish in 26.5 °C water inside of the incubator. The light cycle inside of incubator was controlled following the protocol of cold zebrafish maintenance. Two weeks later, the pigmentation of control zebrafish inside of incubator became slightly pale compared with that outside of incubator but was not severely down-regulated compared with cold zebrafish (Fig. 1A).

Cold exposure disrupts growth of zebrafish

The means and standard deviations of body weight and length were calculated from 6 to 7 zebrafish per group, and Student's *t*-test was used to determine statistical significance. There was a tendency that cold zebrafish had lower body weight and length than normal zebrafish at 1, 2 weeks and 7 months (Fig. 1D). Furthermore, abnormal renal tubules and melanophores were observed in the KM of cold zebrafish, but not in normal zebrafish (Fig. 1E, left and middle panels). To exclude the possibility that the abnormal melanophores were in fact melanin-containing macrophages, images of transmission electron microscopy (TEM) were captured. As shown in Fig. 1E (right panel) and Fig. S2 in Supporting Information, abnormal melanophores are not similar to macrophage in KM, implying that they were not melanin-containing macrophages.

Expression of *csdc2*, *hspa8* and *ef1a* genes in the skin of zebrafish

We next examined whether cold exposure altered the expression of genes encoding cold- and heat-shock proteins, such as *csdc2* and *hspa8*, and elongation factor 1a (*ef1a*), a constitutive gene (Tang *et al.* 2007). Zebrafish were sampled at day 3, 1 and 2 weeks of cold exposure. On day 3, expression levels of *csdc2* and *hspa8* genes in the skin of cold zebrafish were 2.2- and 1.5-fold higher than those of normal zebrafish, respectively (Fig. 2A). After 1 week of cold exposure, expression levels of *csdc2* in cold zebrafish slightly decreased, whereas expression levels of *hspa8* were threefold higher than those of normal zebrafish (Fig. 2A). After 2 weeks of cold exposure, expression levels of both *csdc2* and *hspa8* were not changed. Cold exposure did not alter the expression of *elfa* at all time points, suggesting that cold exposure mainly modulated the expression of *csdc2* and *hspa8*.

Up-regulation of *pmch* and down-regulation of *tyr* and *dct* in cold zebrafish

To understand further how cold exposure down-regulates the pigmentation of zebrafish, we investigated the expression levels of several genes known to be involved in pigmentation. In the brains of cold zebrafish, expression levels of *pomca*, which is involved in melanosome dispersion, were increased at week 1 and then decreased at week 2 (Fig. 2B). *Pmch*, which was involved in melanosome aggregation, remained unchanged at week 1, but increased at week 2 (Fig. 2B). Expression levels of *tyr* and *dct*, which are involved in melanin synthesis, were also investigated. *Tyr* expression was decreased at weeks 1 and 2 of cold exposure, whereas *dct* was decreased at week 1 and then recovered to normal levels at week 2 (Fig. 2B).

We then investigated the expression of genes involved in the differentiation of melanoblasts into melanocytes. *Mitfa*, *kita* and *kitlga* have been identified as indicators for melanocyte differentiation during fin regeneration (Rawls & Johnson 2000). Two weeks after cold exposure, expression levels of *mitfa* and *kita* in the skin of cold zebrafish were not significantly altered compared with normal zebrafish ($P > 0.05$), whereas that of *kitlga* was increased ($P < 0.05$) (Fig. 2C).

Cold exposure reduces the number of melanophores

Our results of morphological observation, melanin content and gene expression enabled us to suggest that the down-regulation of pigmentation in cold zebrafish was caused by (i) down-regulation of melanin synthesis and/or (ii) decrease in the number of melanophores. We then performed histological analyses of skin sam-